EFFECT OF OXIDATIVE STRESS ON KINETIC PARAMETERS OF CELLULAR ACTIN DYNAMICS

By

Sayali Devdatta Kulkarni

RECOMMENDED:

Advisory Committee Chair

Chair, Department of Chemistry & Biochemistry

APPROVED:

Dean, College of Natural Science & Mathematics

Dean of the Graduate School

Dec 13, 2007

Date

EFFECT OF OXIDATIVE STRESS ON KINETIC PARAMETERS OF CELLULAR ACTIN DYNAMICS

A

THESIS

Presented to the Faculty

of the University of Alaska Fairbanks

in Partial Fulfillment of the Requirements

for the Degree of

MASTER OF SCIENCE

By

Sayali Devdatta Kulkarni, M.D.

Fairbanks, Alaska

December 2007

ABSTRACT

The integrity and dynamics of the actin cytoskeleton is essential for the morphology and motility of neuronal cells both in developing and adult nervous system. Oxidative modification of actin both as monomers and in filaments alters the kinetics of actin filament dynamics contributing to neurodegeneration and aging. Our objective focused on changes of the kinetic parameters of oxidized actin as opposed to naive actin and its resulting effects on actin filament dynamics. We first validated Surface Plasmon Resonance (SPR) technology for our objective by studying interaction of naive actin with a monoclonal anti-actin antibody and DNase I. For interactions of actin monomers under polymerizing conditions yet below the critical concentration of actin, we determined real time rate constants for actin nucleation steps for the first time. The association rate constant (k_a) for the first monomer was $7.5x10^3$ $\mu M^{-1}sec^{-1}$ and the dissociation rate constant (k_d) for first monomer was 0.256 sec^{-1}. Whereas K_a for second monomer remained unchanged ($6.66x10^3$ $\mu M^{-1}sec^{-1}$), k_d for second monomer was significantly decreased ($1.82x10^{-3}$ sec^{-1}). We also found that affinity of oxidized actin to unoxidized actin is significantly (100 fold) reduced. Our findings demonstrate that SPR allows measurement of (kinetic parameters) for unmodified actin monomers.

Table of Contents

Page

Page

Page

LIST OF FIGURES

Page

Page

LIST OF TABLES

Page

ACKNOWLEDGEMENT

There are quite a few numbers of people who contributed in some way to this thesis, for which I would like to express thanks.

Foremost, I would like to thank my advisor and committee chair Dr. Thomas B. Kuhn who shared with me a lot of his expertise and research insight. He has been available as a recourse in every way, be it socially, scholarly or administratively. I can not overstate my appreciation to Dr. Marvin Schulte whose thoughtful advice often served to give me the clear sense of direction during this work. He has always been a great source of encouragement and support. I would also like to express my gratitude to committee member Dr. Kristin O'Brien for her constructive comments and department chair Dr. Thomas Clausen for his guidance I want to thank Dr. Jestina Kusina for her assistance during initial stages of the project.

I would like to thank Sheila Chapin, Mist D'June-Gussak and Mary Van Muelken for administrative support. I also wish to thank all my colleagues in both Dr. Kuhn's and Dr. Schulte's laboratories for their support.

I cannot finish without saying how grateful I am to my parents Nilambari and Hemant Tanawade and my brother Mayur Tanawade for their love and support throughout. Finally, yet importantly, I wish to record my sincere appreciation to my husband Dr. Devdatta Kulkarni who has been a great source of strength all through this work. I dedicate my thesis to him.

CHAPTER ONE

Physiology of Actin Dynamics

1.1 Introduction

Actin is one of the most abundant intracellular proteins in eukaryotic cells. Actin, microtubules and intermediate filaments make up the cytoskeletal system of cells. Depending on the cell type, actin (either monomeric or filaments of both) accounts for 5-10% of the total protein. For example, in muscle cells, 10 % (by weight) of the total cellular protein is actin (Degen et al, 1983). The cytosolic concentration of actin in non-muscle cells ranges from 0.1 to 0.5 mM. In special structures such as microvilli or lamellipodia, the local actin concentration can be as high as 5 mM.

1.2 Sequence Homology

Actin is one of the most conserved eukaryotic proteins with a degree of conservation comparable to histones, the structural proteins of chromatin, that are known to have 96-98% conservation of sequence. Actin arose from an ancestral bacterial gene and further evolved as eukaryotic cells became more specialized. A comparison of primary structures of over 30 actin isotypes shows that a maximum of 32 out of 375 total amino acid residues can be substituted. The isoform variations are tissue-specific and species-independent. Only 25 residues differ among the most diverse isoforms. Large segments of the sequence, including amino acids 19-75 and 307-375 are highly conserved with very minor exceptions. Nine substitutions confined to the N terminal 18 residues, 10 substitutions between residues 260-306 and 13 more substitutions within the remaining regions. Overall the conservation percentage is about 96 % (Hambly et al, 1972).

1.3 Isoforms

Some single celled organisms such as yeast have one or two ancestral actin genes. Humans have six genes encoding six isoforms of actin. In vertebrates, four actin isoforms

are present in muscle cells and two isoforms, β-actin and γ-actin, are present in non-muscle cells. The six isoforms differ in 25 amino acid residues out of 375 amino acids residues. Different isoforms may have different functions. For example, α-actin is associated with contractile structures, while β-actin is found mostly within the cell cortex and at the leading edge of motile cells. Actin protein exists in two forms:

- G-actin or globular or monomeric form (hence forth referred to as G-actin)
- F-actin or filamentous or polymeric form (hence forth referred to as F-actin)

1.4 G-actin Structure and Properties

G-actin is a polypeptide chain of 375 amino acids with a molecular weight of 43,000 Dalton.

Figure 1.1 3-Dimensional Structure of Actin-Profilin Complex (NCBI PDB 2BTF)

The actin monomer assumes a compact globular form and measures approximately 5.5x5.5x3.5 nm. Each G-actin binds one molecule of either ATP or ADP. It has one high affinity and several low-affinity binding sites for divalent cations. Tightly bound cations are directly associated with the phosphates of nucleotide. In the absence of cations, actin is unstable and denatures rapidly.

Each actin monomer contains both a small and a large domain separated by a central cleft with a flexible hinge region. Each of those domains can be further divided into two sub-domains, giving rise to four globular lobes. Both the amino and carboxyl termini are located within the small domain. The ATP binding site is located in the bottom of the cleft between the two domains. The cation is positioned within a hydrophilic pocket close to the nucleotide-binding site such that the pocket is closed off from the top by the di- or tri- phosphate moiety of adenine. Salt bridges and hydrogen bonds involving adenine phosphates stabilize the association of the two domains (Holmes and Kabsch 1991).

The actin cytoskeleton can be arranged into many different structures, depending on the requirements of the cell. Actin filaments are organized both by actin binding and regulatory proteins. In this process actin not only binds to other proteins but also to itself to form a highly dynamic actin filament.

1.5 Actin Dynamics

Actin monomers have the tendency to aggregate both *in vitro* and *in vivo* into a network of actin filaments. The equilibrium between actin in its monomeric and polymeric form is highly dynamic. Actin filaments are continually growing or shrinking. These changes in organization generate force, which in turn can change the shape of the cell or support directional cell motility.

The rate at which G-actin subunits are added to the filament end is called the on rate or the rate of association. The rate at which actin monomers depolymerize from the filament ends is called off rate or the rate of dissociation. Both the rates are different for each end of the actin filament. The barbed, or plus, or positive, or fast-growing end (henceforth refereed to as fast-growing end) exhibits a faster on-rate and a slower off-rate compared to the other i.e. slow-growing end. The fast-growing end kinetically contributes to the formation of filaments. The association rate constant of G actin-ATP at the fast growing end is 11.6 $\mu M^{-1}sec^{-1}$ and the dissociation rate constant is 1.3 $\mu M^{-1}sec^{-1}$ (Carlier and Pentaloni, 1997). The other end with slower association and faster dissociation rates is also referred to as the minus end, or negative end, or slow-growing end (henceforth refereed to as slow-growing end). In other words, the critical concentration for the fast-growing end is lower than that for slow-growing end. The association rate constant of G actin-ATP at the slow-growing end is 1.4 $\mu M^{-1}sec^{-1}$ and the dissociation rate constant is 0.8 $\mu M^{-1}sec^{-1}$.

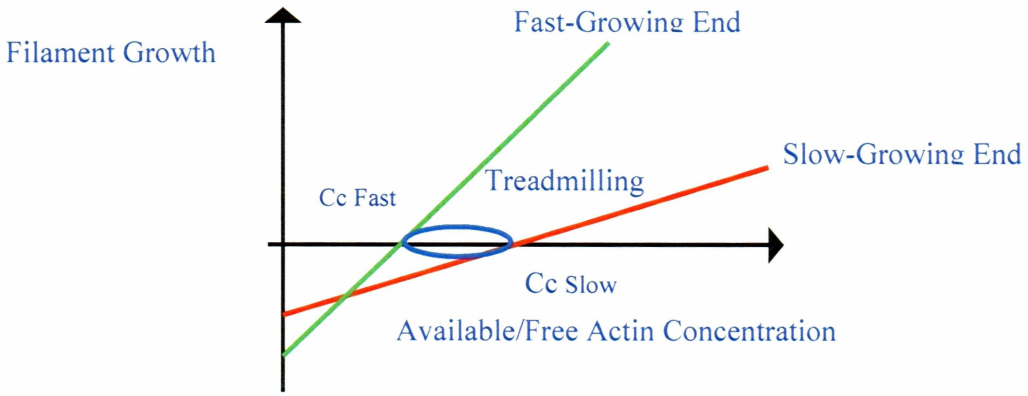

Figure 1.2 Concentration of Available Actin Determines Filament Formation

Thus, four different species of actin molecules occur in cells depending on its polymerization status and whether ATP or ADP is bound. These are G-actin-ATP, F-actin-ATP, F-actin-ADP and G- actin-ADP.

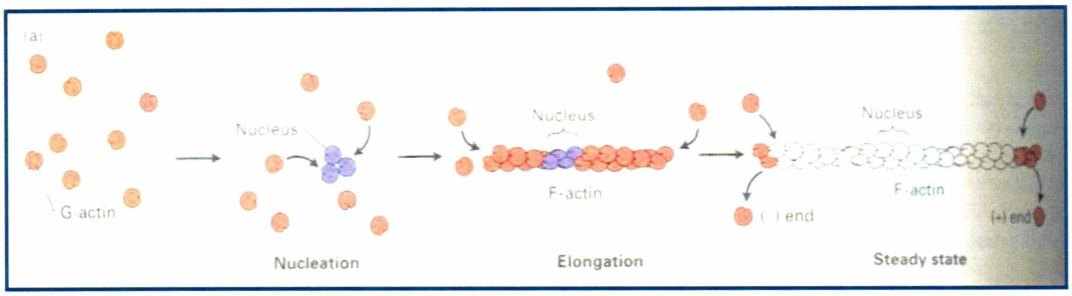

Figure 1.3 Actin Filament Formation (Molecular Biology of the cell, Lodish et al, Fifth Edition)

1.6 Actin Polymerization *in vitro*

The polymerization process can be divided into three phases. The first phase is nucleation, which describes the initial formation of three assembled actin monomers. Nucleation is slow because it is thermodynamically unfavorable to orient three protein molecules. This phase is also rate limiting and is referred to as the lag phase. *In vivo*, Arp2/3 accelerates this phase by mimicking the actin nucleus. *In vitro*, this initial lag phase can be eliminated by the addition of F-actin nuclei to the solution of G-actin.

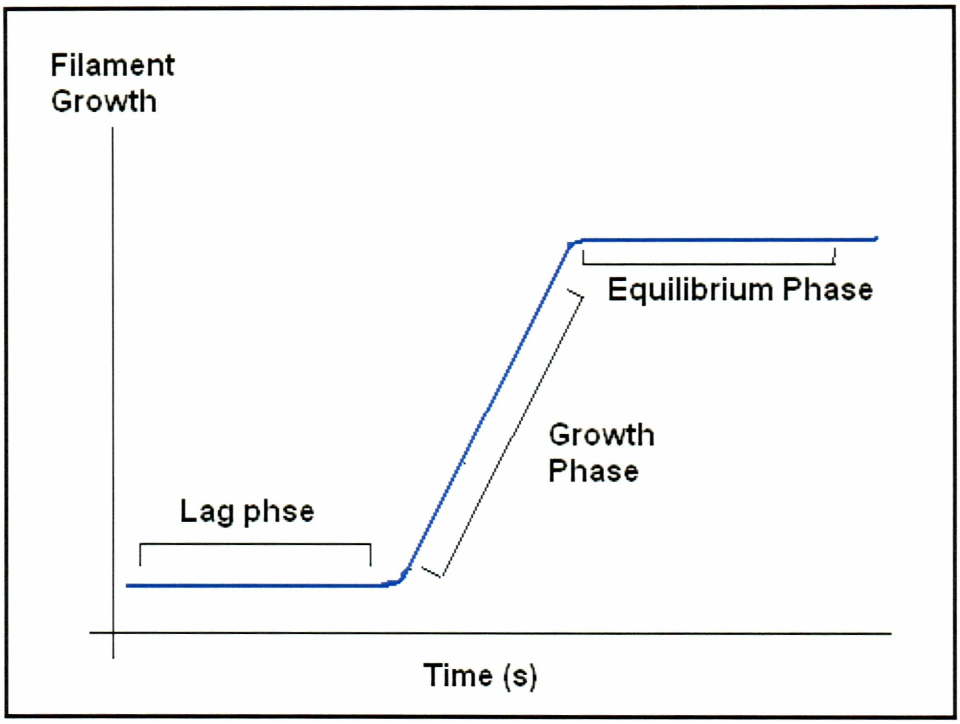

Figure 1.4 Phases of Actin Polymerization.

The second phase of filament formation is called the growth phase. Once the nucleus is formed, the filament grows through the addition of monomers to each end. As the filament grows, the concentration of G-actin-ATP decreases until equilibrium is reached between assembly and disassembly of F-actin. As F-actin-bound ATP becomes hydrolyzed, the F-actin loses stability and G-actin dissociate from the slow-growing end. The association of G-actin at the fast-growing end balances the rate of dissociation of the G-actin from the slow-growing end. This point of equilibrium is distinct for the fast-growing and slow-growing ends. In this steady state phase, G-actin monomers exchange with subunits at the F-actin ends and there is no net change in the total mass of the filament. As a result, the length of the filament remains constant but the individual actin monomers undergo retrograde flow towards the pointed end of the filament. This stage is also called as treadmilling. When the G-actin-ATP concentration is between the critical concentrations for the fast- and slow-growing ends, actin subunits are added to the fast-growing end and dissociate from the slow-growing end. If the concentration of actin is

above the critical concentration for both ends then the filament grows at both ends. However, when the concentration of G-actin-ATP reaches the critical concentration of fast-growing end, filament growth stops.

Assembly of G-actin molecules into F-actin begins with the binding of ATP to G-actin. The critical concentration refers to the minimal concentration of free soluble G-actin and is approximately 2-5 μM. Below this concentration, G-actin binds other G-actin but cannot form F-actin. *In vivo*, the actin-binding protein thymosin sequesters G-actin and effectively lowers the concentration of available G-actin-ATP. Profilin on other hand lowers the critical concentration by enhancing nucleotide exchange of G-actin. *In vitro*, in the absence of actin binding proteins, the critical concentration remains constant.

1.7 Actin Polymer

The formation of the actin filament stimulates ATPase activity within actin. The phosphates are released more slowly from a newly formed filament than a mature filament. Hence, the growing filament has a cap of ATP-actin at its fast-growing end followed by a zone that contains G-actin-ADP and phosphate. Mature filaments contain more ADP-actin species.

F-actin appears as two helical strands of subunits that cross each other every 35 nm (helix pitch). One pitch consists of 28 subunits, 14 in each strand, covering a distance of 72 nm. Because of the twists, the filament appears alternately thinner (7 nm) and thicker (9 nm) (Bramer and Aebi, 1992). Each actin monomer binds to four others within each filament with one subunit above, one subunit below, and two subunits on either side. The actin monomers are joined by two different bond types:

- Relatively strong bonds between monomers along a single helix
- Relatively weak bonds between monomers on opposite strands.

All subunits within the filament point toward the same end of the filament. This is consistent with the polarity of individual G-actin molecules. The nucleotide-binding site

is exposed on the slow-growing end of the filament. Consequently, the filament exhibits polarity i.e. one end differs from the other just like the G-actin molecule. The polarity of the filament has been determined in myosin decoration experiments using electron microscopy. This method exploits the ability of myosin to bind specifically to actin filaments. Myosin attaches to the sides of each filament with a slight tilt. When myosin is bound to all actin subunits, the filament appears decorated with arrowheads pointing towards the slow-growing end of the filament. Hence, the slow-growing end is also called the pointed end and the fast-growing end is also called barbed end.

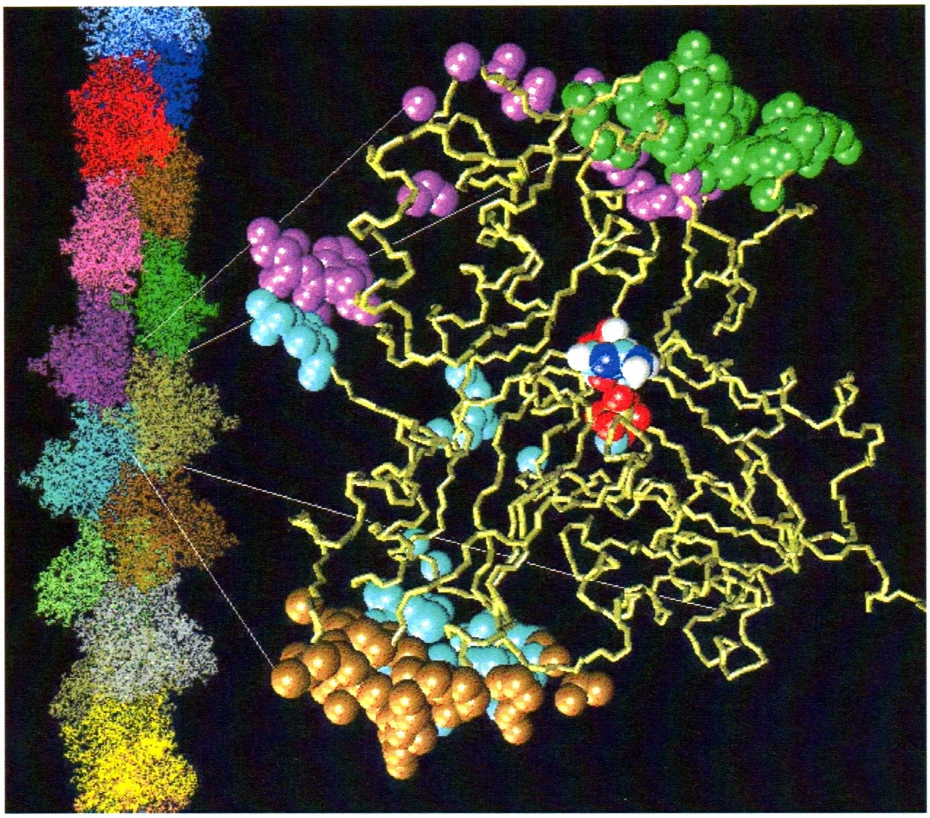

Figure 1.5 Lorenz model of F-actin. The entire F-actin is shown on the left while a single G-actin monomer with inter-actin contact surfaces is shown on the right.
Source: Wriggers and Schulten, 1997, Biophysical journal, volume 73, 624-639

1.8 Cellular Location

Actin filaments assemble into many different superstructures within the cell. Each of these superstructures serves a specific cellular function. Figure 1.6 shows the location of superstructures formed by actin in a neuronal growth cone. The growth cone is the most distal part of a growing or migrating neuron. This structure is highly motile and this motility is supported by specialized structures formed of actin. Actin filaments exist in tight bundles that form finger-like cell surface projections known as filopodia. Similar structures in non-neuronal cells are called as microvilli or pseudopodia, which are relatively shorter than filopodia. Lamellipodia are a less ordered structure in which actin forms a gel-like meshwork. In epithelial cells, actin filaments form contractile bands called adherent belts. In many cells, actin filaments form contractile stress fibers that assist adhesion to substrates via focal adhesion clusters. During cytokinesis, a contractile ring composed of actin and myosin separates the two daughter cells. Actin filaments are molded into these various structures by numerous different actin-binding proteins. Along with other functional proteins, cells can harness the power of actin polymerization to do work. The actin cytoskeleton can also be used as a walking track to guide myosin motor proteins.

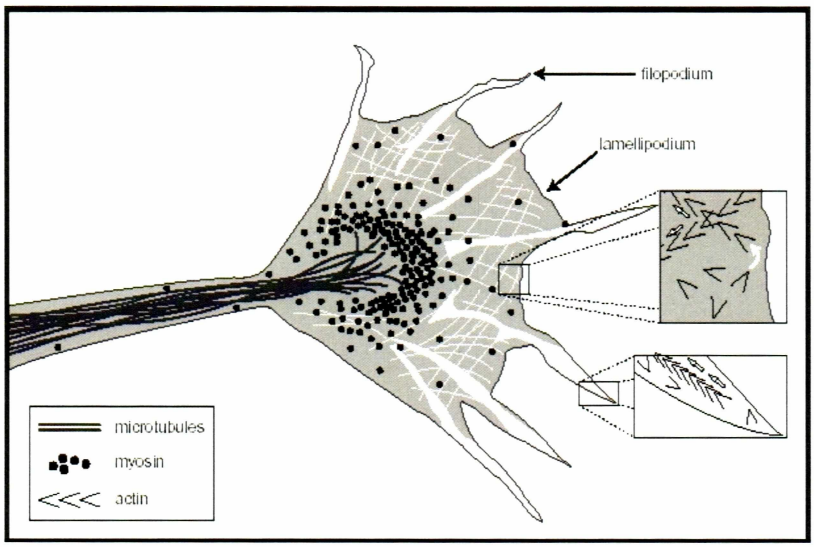

Figure 1.6 Cellular Locations of Actin. Reference: Luo 2002, Annual Review in Cell and Developmental Biology, 18:601-635

Even though the concentration of monomeric actin in cells is considerably higher than the critical concentration of both ends, only 50% of actin molecules are found in the filamentous state. Actin monomers are sequestered by an important actin regulatory protein, thymosin. When a cell is in need of actin filaments another actin regulatory protein, profilin, stimulates the release of actin monomer from thymosin and facilitates polymerization. This process allows cells to rapidly alter motility and morphology in response to extrinsic stimuli.

1.9 Profilin and Cofilin

Measurements of actin turnover rates are 100 times faster *in vivo* than *in vitro*. Treadmilling rates *in vivo* are enhanced by two important actin-binding proteins, cofilin and profilin. Because of these two functional proteins, cell can recharge the ADP-actin dissociated from the slow-growing end to ATP-actin at the fast-growing end.

Profilin is a small protein (molecular weight about 33000 Dalton) that binds to G actin on the side opposite of the nucleotide-binding site. Profilin binding facilitates the opening of the cleft and increases the rate of ADP release and ATP binding. The profilin-actin-ATP complex does not bind the minus end of actin filaments because profilin blocks the binding site. It efficiently binds to the positive end. Once the new actin subunit is bound, profilin dissociates from the actin. This mechanism provides a constant supply of actin-ATP for released Actin-ADP. Consequently, all the G actin in the cell has bound ATP.

Cofilin is a protein that binds specifically to F actin-ADP at the association site between two actin monomers within the filament and induces a small twist. Cofilin also binds cooperatively. It alters the helical twist by 5° per subunit and shortens crossover. As a result, the actin filament is destabilized and severs. Thus, cofilin generates multiple short actin fragments from an existing filament. Released actin-ADP subunits are recharged by profilin through the mechanism discussed above. ADP/cofilin also greatly

enhances the off rate of actin-ADP and tightly binds to ADP-G-Actin thus preventing nucleotide exchange. Together, profilin and cofilin enhance treadmilling rates up to 30 fold *in vivo*, compared to levels *in vitro*.

1.10 Thymosin

Cells often contain a very large pool of unpolymerized actin. The average cellular concentration of G-actin is approximately 50-200 μM. The critical concentration of actin on the other hand is only about 2-5 uM *in vivo*. The activity of actin monomer sequestering proteins, especially thymosin, maintains G-actin in the monomer state. Thymosin-β4 binds to ATP-G-actin and inhibits the addition of the actin subunit to either end of the filament. Thymosin is usually found at high concentration in cells that have a high actin concentration such as human thrombocytes and platelets. Thymosin buffers the pool of unpolymerized actin as needed by the cell.

1.11 Capping Protein Gelsolin

This class of proteins binds to the positive end of filaments and also severs actin filaments. Gelsolin is an important member of this family. Gelsolin is regulated by intracellular Ca^{2+} levels. Upon binding Ca^{2+} it undergoes a conformational change that exposes the actin-binding site. Gelsolin binds between the actin molecules of the helix and breaks the filament. It then remains bound to the fast-growing end of the filament and exposes a new slow-growing end that can disassemble. Actin cross-linking proteins such as formin can turn the solution of actin into a gel. Under conditions with elevated intracellular Ca^{2+} levels, gelsolin breaks the filaments and converted the gel into solution again. Hence, the name is given as Gelsolin.

1.12 WASp and Arp2/3

Nucleation is the rate-limiting step of actin polymerization both *in vitro* and *in vivo*. Actin nucleating proteins assist in nucleation and thus are important modulators of actin function. Arp2/3 is the most important member of this class. It consists of seven subunits.

Two of them are Actin Related Proteins (Arp2/3). This complex is activated by another protein, Wiskott-Aldrich syndrome protein (WASp) and by preformed actin filaments. WASp in turn is activated by cell signaling cascade. Arp2/3 binds at a 70° angle to the side of an actin filament and mimics the positive end of the filament. This provides a template for the assembly of a new filament. This new end grows as long as G-actin-ATP is available, or until it is capped by actin capping proteins. Thus Arp2/3 complex is used to drive actin polymerization and to power cellular motility.

Extracellular signals are transmitted across the plasma membrane by receptors specific for different factors. One set of growth factors induces actin polymerization at the leading edge through a Rac-and Cdc42-dependent pathway. A small Ras-related GTP-binding protein Cdc42 activates WASp. Under normal conditions, WASp exists in a folded inactive conformation. In this inactive state the Arp2/3 activating domain is not available for binding to actin. Cdc42 binds to GTP and help opening the folded conformation of WASp thus activating it. Other than activating Arp2/3 to bind to actin, WASp can also bind to actin itself. Thus the stepwise activation of Cdc42, WASp and Arp2/3 drives actin polymerization and powers cellular motility.

CHAPTER TWO

Oxidative Stress and Oxidative Modifications

2.1 Introduction

Reactive oxygen species (ROS) arise in cells and tissues as byproducts of many endogenous and exogenous sources including UV light, radiation, neutrophil activity, various enzyme reactions, and metabolism. Emerging evidence demonstrates that ROS and reactive nitrogen species (RNS) have important roles in physiological functions. They are also involved in the initiation and/or progression of many pathologies. The balance between the physiological versus pathological contribution of ROS is determined by the relative rates of formation and removal of these species. Normally cells rapidly remove ROS and RNS before they damage cells. An imbalance between the production of ROS or RNS and the antioxidant defense capacity leads to oxidative or nitrosative stress and damage to proteins, lipids, nucleic acids and carbohydrates (Dalle-Donne et al, 2005). High levels of ROS/RNS induce distinct pathological consequences. It results in amplification and propagation of cell and tissue degeneration making it irreversible. Protein oxidation has also been shown to accelerate ageing (Droge 2003).

2.2 Sources of Reactive Oxygen Species and Reactive Nitrogen Species (ROS and RNS)

Mitochondria are the major source of cellular ROS. Oxidative phosphorylation produces potentially toxic oxygen metabolites. The electron transport chain in the mitochondria transfers redox energy from NADH and $FADH_2$ to oxygen (O_2) in several steps. These energy-rich molecules are produced within the matrix of the mitochondrion via the citric acid cycle. They are also produced in the cytoplasm by glycolysis. Their reducing equivalents are imported from the cytoplasm via the malate-aspartate shuttle system of antiporter proteins. They can be fed into the electron transport chain using a glycerol phosphate shuttle. Protein complexes in the inner membrane (NADH dehydrogenase, cytochrome c reductase and cytochrome c oxidase) perform the transfer and the release of

energy which is then used to pump protons into the intermembrane space. This process is efficient but a small percentage (1%) of oxygen is incompletely reduced to water. Disruption in electron transport can also increase superoxide production. Superoxide is converted into H_2O_2 and O_2 by superoxide dismutases (SODs). H_2O_2 can react with transition metals such as copper (and more often iron) to produce highly reactive hydroxyl radicals ($HO^{\cdot}$). Alternatively, H_2O_2 can be converted to water by the enzymes catalases and glutathione peroxidase. H_2O_2 produced by inflammatory cells oxidizes enzyme myeloperoxidase to a higher oxidation state. This complex oxidizes chloride ions to hypochlorous acid (HOCl). Hypochlorous acid can then oxidize or chlorinate cellular molecules. HOCl especially reacts with methionine residues and thiols. Oxidative damage to mitochondria may contribute to their declined function and is thought as an important factor in aging.

An important source of ROS is the membrane-bound enzyme NADPH oxidase (Thannickal and Fanburg 2000). These enzymes generate ROS species as their primary product, which have important roles in regulation of numerous physiological processes including cell signaling, gene expression and phagocytosis. Isoforms of NADPH oxidase are found in all types of cells. NADPH oxidase is a multi-subunit protein complex. The activity of this multi-protein enzyme is dependent on the regulated assembly of the six enzyme subunits at the plasma membrane. They associate in a stimulus-dependent stimulus-dependent manner to form the active enzyme complex. In phagocytic cells in particular, this activity has to be spatially and temporally restricted to the closed phagosome in order to prevent destruction of host tissue. The regulation of enzymatic activity is achieved by two mechanisms: separation of the oxidase subunits into different subcellular locations during the resting state (cytosolic and membrane-bound) and modulation of reversible protein–protein and protein–lipid interactions. These can either enforce the resting state or allow translocation to the membrane in response to the appropriate stimulus. The flavocytochrome b558 lies at the core of the catalytic site. It is formed by the association of a large glycoprotein, gp91phox (phox for phagocyte

oxidase) known as the β subunit, and a small subunit p22 phox, known as α subunit. This core exists in a dormant state in the absence of the other subunits. $gp91^{phox}$ and $p22^{phox}$, are integral membrane proteins. All gp91 isoforms are members of the NOX family. NOX2 is the classic phagocyte flavoprotein. Other components exist as cytosolic proteins in the resting state and act as regulatory subunits. These include p67phox, p47phox, p40 phox and Rac1, which upon translocation to the cytoplasmic side of the plasma membrane associate with membrane subunits thus assembling functional NOX complex (Groemping and Rittinger 2005). Those subunits are maintained in the cytosol, either through auto-inhibitory interactions or through complex formation with accessory proteins that are not part of the active enzyme complex. Multiple inputs are required to disrupt these inhibitory interactions and allow translocation to the membrane and association with the integral membrane components.

Electrons are transferred from intracellular NADPH onto extracellular oxygen through a redox chain within the enzyme resulting in superoxide radical. Resultant depolarization of the membrane is compensated by proton flux through the membrane. Along with NADPH oxidase, the plasma membrane, mitochondria and Golgi all contain a lipophilic coenzyme Q (CoQ or ubiquinone). CoQ is an intermediate electron carrier that shuttles electrons from intracellular nucleotides to extracellular oxidants and thus functions as an important antioxidant.

Reactive Nitrogen Species (RNS) such as nitric oxide (NO), nitrite and peroxyinitrite ($ONOO^-$) are similar to ROS. They are physiologically important but at high levels, potentially destructive. Nitric oxide is generated from the NADPH-dependent oxidation of arginine, which is catalyzed by nitric oxide synthatases. $NO^·$ reacts rapidly with heme prosthetic groups and thiols. Most importantly, it reacts with superoxide to form peroxynitrile. When $NO^·$ concentrations increase in cells to levels within the range of SOD, $NO^·$ competes with SOD for the removal of superoxide anions, which leads to the formation of peroxynitrite ($ONOO^-$). Thiol modifications are the most adverse effects

of peroxinitrite. Oxidized NO· derived species ($ONOO^{-}\cdot$, NO_2 and N_2O_3) readily react with glutathione to form nitrosated thiols(Dalle-Donne et al, 2003).

2.3 Oxygen Free Radicals

Free radicals are chemical species with one or more unpaired electrons. Free radicals combine with the atom of hydrogen (one unpaired electron), most transitional metal ions, and the oxygen molecule. O_2 in its ground state is a radical with two unpaired electrons. O_2 readily reacts to form partially reduced species, which are generally short-lived and highly reactive, and thus are called as reactive oxygen species. Some relevant ROS include:

The superoxide anion ($O_2^{-}\cdot$) is formed through one electron reduction of O_2^{-}.

$O_2 + e^{-} = O_2^{-}\cdot$

Hydrogen peroxide has (H_2O_2) no unpaired electrons. Thus, it is not radical. It is formed by several metabolic reactions such as the dismutation reaction of O_2^{-} catalyzed by superoxide dismutase. This reaction produces the hydroperoxyl radical as an intermediate. The hydroxyl radical (·OH) can be formed either by superoxide ion or from H_2O_2.

$$O_2^{-} - + H_2O_2 \rightarrow O_2 + HO - + \bullet OH$$

(Haber – Weiss)

$$Me^{n+} + H_2O_2 \rightarrow Me^{(n+1)+} + HO - + \bullet OH$$

Here Me^{n+} is a metal ion. The most frequent reaction is the iron-catalyzed decomposition of H_2O_2. Hydroxyl radical (·OH) is the most toxic form of oxygen. It is highly reactive and reacts indiscriminately with molecules in close proximity to where it is produced. Thus it is unlikely to function as signaling molecule. Both H_2O_2 and $O_2^{-}\cdot$ are less reactive and longer-lived compared to the hydroxyl radical and are more likely to function as intracellular and intercellular signaling molecules (Moldovan and Moldovan, 2004).

2.4 Defense Against ROS/RNS

Naturally occurring enzymatic and non-enzymatic systems exist to protect cells and tissues against continuous production of ROS/RNS during normal metabolism. These include antioxidant enzymes such as catalases, superoxide dismutases, peroxiredoxins and glutathione peroxidases. Ferritin and ceruloplasmin are two important non-enzymatic proteins that defensd against ROS/RNS,in body fluids. Ferritin binds iron and ceruloplasmin binds copper. These two proteins are involved in metal catalyzed auto-oxidation. These reactions lead to OH production from superoxide. Other important antioxidants are α-tocopherol (vitamin E), ascorbic acid (vitamin C) and glutathione (L-γ-glutamyl-L-cysteinyl-glycine).

Thiol antioxidants are an important family of antioxidant molecules. This includes reduced glutathione (GSH) and -SH molecules such as N-acetyl cysteine (NAC). NAC shares a free -SH group with GSH. It also serves as a precursor of GSH. One major function of GSH is detoxification of peroxides through the action of GSH peroxidases (GSH Px). The resulting GSSG is reduced by GSSG reductase (GR). GSSG can also glutathionylate protein cysteines (PSH) to mixed disulfides (PSSG, glutathionylated protein). Glutathionylation is reversible and PSSG can be reduced by glutaredoxin (Grx). Thus GSH represents a redox buffer in the cell. The reduced/oxidized ratio of glutathione defines the redox state of the cell (Fratelli et al, 2004).

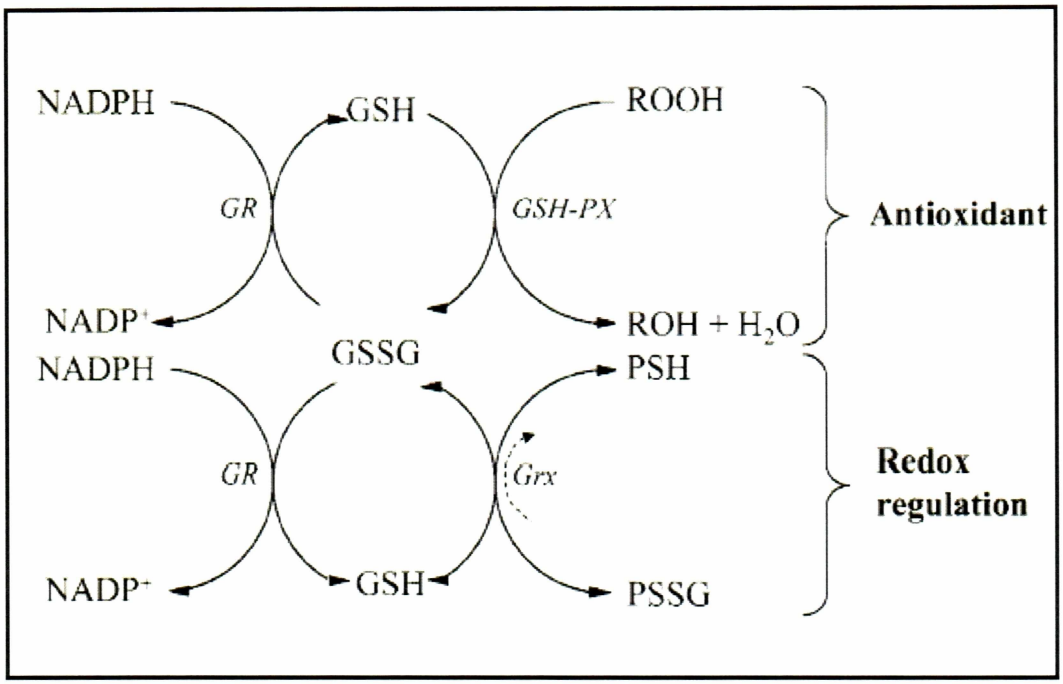

Figure 2.1 Dual Role of Glutathione in Redox Environment

Source: Pietro and Bonetto, Redox Proteomics, 2003, 3, 1145-1153

2.5 Oxidation of Biomolecules and Aging

Aging is associated with an accumulation of oxidatively modified proteins (Berlett and Stadtman, 1997). Studies have shown protein carbonyls increase with age in the brain and fibroblasts cells. Moreover, injections of free radical scavengers leads to reversal of some age related changes in brain and discontinued treatment results in reappearance of these ages-related changes (Stadtman 2006).

2.6 Oxidative Modifications of Proteins

High levels of ROS/NOS and/or impaired antioxidant enzyme systems lead to the formation of chemically modified proteins. Irreversible modifications such as lysine and arginine carbonylation, tyrosine and tryptophan nitration, dityrosine formation, sulfhydryl oxidation to sulfenic/sufinic/sulfonic acid, and protein-protein cross-linking generally result in permanent loss of function of oxidized proteins. These proteins are subsequently

degraded, but can also accumulate in the cytoplasm as insoluble inclusions that are characteristic of many neurodegenerative diseases (Ghezzi and Bonetto, 2003). On the other hand, some oxidative modifications are reversible, such as glutathionylation, and -nitrosylation. These types of modifications may have a role in redox regulation of proteins or enzymes.

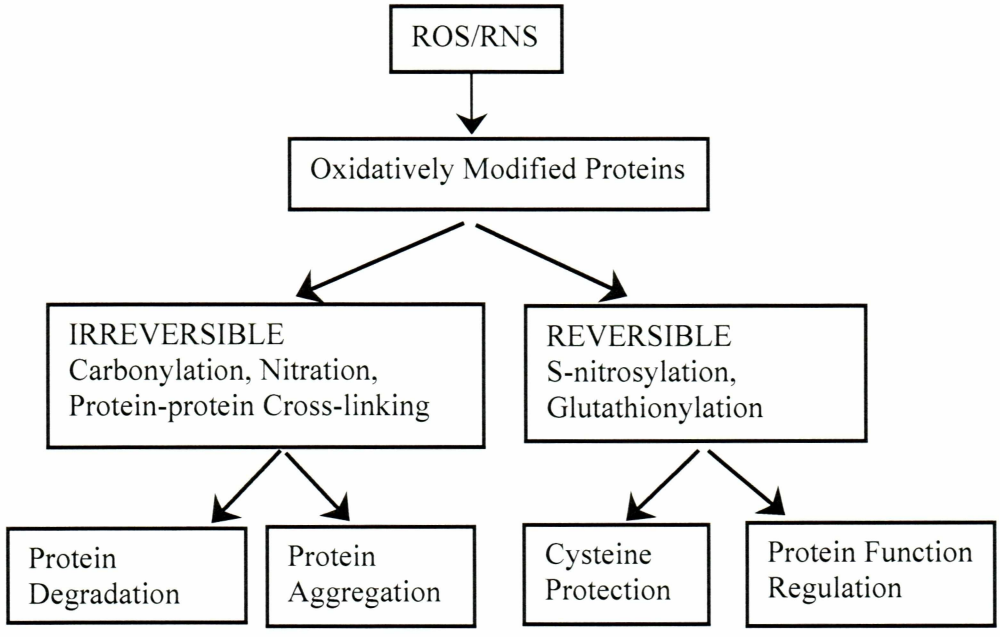

Figure 2.2 Types of Protein Modifications. ROS/RNS can lead to reversible or irreversible protein modifications as shown above.
Source: Pietro and Bonetto, Redox Proteomics, 2003, 3, 1145-1153

2.7 Carbonylation

Protein carbonylation is one marker of ROS-mediated protein oxidation. Elevated protein carbonyls are associated with aging and disorders such as neurodegenerative diseases and ischemic stroke. Carbonyl groups may be introduced to a protein at various sites and by different mechanisms (Dalle-Donne 2006).

1. Protein carbonylation can occur at the protein backbone via direct oxidation. This leads to formation of protein fragments with N terminal α-ketoacyl amino acid side chains.
2. Oxidation of some amino acids, particularly histidine, arginine, and lysine residues which leads to the formation of ketones or aldehydes.
3. Proteins can also react with products of lipid peroxidation
4. Conjugation with reduced carbohydrates and their oxidation products.

2.8 Tyrosine Nitration

Nitration of tyrosine to 3-nitrotyrosine is an indicator of peroxinitrile formation and irreversible protein damage. Increased nitrotyrosine levels have been detected in several pathologies including Alzheimer's disease, amyotropic lateral sclerosis, Parkinson's disease, etc. Peroxinitrite is a potent oxidant formed by the reaction of nitric oxide with superoxide. Tyrosine nitration has been found to have role in cell signaling. Peroxynitrite-mediated nitration of a single tyrosine residue in purified cdc2, a cell cycle kinase, prevents its phosphorylation on tyrosine preventing further kinase activity (Kong et al, 1996).

2.9 Thiol Oxidation

Thiols can be irreversibly oxidized to sulfinic ($P\text{-}SO_2H$) (P represents Protein) and cysteic acids ($P\text{-}SO_3H$). Some forms of thiol oxidation are reversible and are involved in the redox regulation of proteins. These include the formation of nitrosothiols (P-SNO), sulfenic acids (P-SOH), and thiol radicals (P-S). Redox regulation is mediated by formation or reduction of disulfides and mixed disulfides with small molecular weight thiols, especially GSH. Targets of redox regulation are cytoplasmic proteins that can undergo oxidation and not the protein occurring in oxidized state and undergoing reduction.

2.10 Glutathionylation and Cysteinylation

The formation of mixed disulfides occurs by sulfhydryl oxidation or by thiol disulfide exchange.

$$PSH + GSH + H_2O_2 \rightarrow PSSG + H_2O$$

$$PSH + GSSG \rightarrow PSSG + GSH$$

PSSG formation can also be promoted by nitric oxide formation. Intracellular disulfides can be reduced by thioredoxin. Mixed disulfides with glutathione are reduced by glutaredoxins.

2.11 S-Nitrosylation

S-nitrosylation is the covalent attachment of a nitrogen monoxide group to the thiol side chain of cysteine. This is an important mechanism by which nitric oxide modulates the activity of proteins. This reaction is reversible under many conditions. Nitrosothiols can also be reduced by ascorbic acid, GSH and thioredoxin.

CHAPTER THREE

Oxidative Modifications of Cellular Actin Cytoskeleton

3.1 Introduction

An imbalance between ROS production and the antioxidant capacity of the cell results in oxidative stress. Oxidative stress can result in adaptation phenomena such as induction of antioxidant defenses or heat shock proteins or cell injury. The response to injury can be reversible where the cell enters a temporary or prolonged altered steady state, and does not die. Reversible responses can be part of early events in response to an oxidative insult. If the cell is exposed to severe oxidative stress, it may die. Oxidative stress can cause damage to all types of biological molecules, DNA, proteins and lipids. The primary cellular target of oxidative stress varies depending on the cell type, the nature of stress, its site of generation, the proximity of the oxidant to a specific cellular substrate and the severity of the stress. In mammalian cells, a variety of extracellular stimuli such as cytokines and growth factors, produce a transient burst of oxidants resulting in oxidative stress and oxidative damage of biomolecules. Studies have shown that oxidative stress in cells is usually expressed as free-thiol oxidation, appearance of oxidized proteins, disassembly of cytoskeleton, depletion of pyridine nucleotide and ATP pools, increased plasma-membrane peroxidation and permeability, release of cytosolic components, elevation of free Ca^{2+} and breaking of DNA strands (Dalle-Donne et al, 2001). The dynamic reorganization of cellular actin is highly regulated and ROS appear to play an important role in this process.

3.2 Redox Regulation of Actin Cytoskeleton

Rac1 is a small GTPase that is involved in activating the NADPH oxidase and reorganizing the actin cytoskeleton. Goldschmidt-Clermont and Moldovan (1999) first proposed that there might be link between superoxide generation by NADPH oxidase and remodeling of actin cytoskeleton mediated by Rac1. In posthypoxic endothelial cells, a

condition was found to induce xanthine oxidase mediated production of O_2 simultaneously increasing the pool of filamentous actin. This effect was reversed by over-expression of superoxide dismutase. This suggested that O2 ˙⁻could be involved in actin control. ROS production and membrane ruffle formation is elevated in endothelial cells overexpressing Rac1. Both of these effects are reversed by the addition of antioxidants (Goldschmidt-Clermont and Moldovan, 1999).

Growth factor and cytokine-mediated signal transduction leads to the generation of intracellular H_2O_2. H_2O_2 is generated transiently upon activation of growth factor and cytokine receptors and serves as an effective second messenger. Its spatiotemporal presence in cells correlates with alternation in actin microfilament organization.

In order to play a role in signaling to the microfilament system, the site of production of H_2O_2 must be localized near the actin cytoskeleton. Efficient reduction systems in the cell such as glutathione peroxidase, peroxiredoxins and catalase rapidly eliminate H_2O_2 and must be overwhelmed for H_2O_2 to function in cell signaling. A gradient of H_2O_2 may also have differential oxidative effects of functional relevance, leading to different actin structures depending on the location of the actin molecules, the source of the oxidant, the availability of surrounding reducing systems, and the presence of glutathione. The major sources of ROS within both phagocytotic and non-phagocytotic cells are NAD(P)H oxidase-like protein complexes and lipoxygenase complexes functioning downstream of cytokine receptors. These enzyme complexes are membrane-associated and activated by association with the GTPase Rac. Rac serves as a pivotal regulator of actin assembly and seems to determine where and when actin polymerizes. Amplification of an H_2O_2 signal seems to occur through the integration of the Rac and phosphatidylinositol lipid kinase pathways.

ROS can regulate cytoskeletal dynamics through direct or indirect systems. Indirect regulation is achieved through soluble redox sensitive enzymes whose oxidation

gives rise to a signal culminating in cytoskeleton reorganization. Direct regulation is gained through direct oxidation of actin.

3.3 Covalent Modifications of Actin

Actin is a direct target for oxidative modification *in vivo*. Actin is oxidatively modified in variety of pathophysiological states. This suggests that oxidation might have a casual role in mechanical dysfunction of actin dynamics. The explanation of the molecular basis of this redox regulation requires understanding of the mechanism of the assembly /disassembly and related changes in redox environment. Most of the research has focused on characterizing actin under reducing conditions. It is equally important to understand its properties under oxidizing conditions as representative of the circumstances during signal transduction by H_2O_2.

3.3.1 Cysteine Modifications

Oxidative modifications of cysteines in response to transmembrane signaling have emerged as a regulatory and reversible mechanism of central function in a wide variety of systems. In bacterial oxidative stress-responsive protein OxyR, formation of intramolecular disulfide bridges leads to its activation (Christman et al, 1985). In the nucleus, the reduced state of critical cysteines in some transcription factors, facilitated by disulfide reducing systems such as thioredoxin and redox factor-1, appears to promote DNA binding and transactivation (Hirota et al, 1999). Figure 3.1 shows position of cysteine residues in the G-actin molecule. Skeletal muscle actin contains five cysteines, at positions 10, 217, 257, 285 and 374. Actin contains 6 highly conserved cysteine residues, the sixth being at position 272. The three-dimensional structure reveals that only the thiol of the cysteine in the position 374 is exposed on the surface of the protein and is highly mobile. The surface exposure of this thiol is not affected by incorporation of actin monomer into actin filament. Hence it is vulnerable for oxidative modification in both the monomeric and polymeric state of the protein. Cys374 also has an important role in establishing inter-monomer contacts. During polymerization, Cys374 on one monomer is

near residue 41 in subdomain 2 (part of larger domain of G-actin molecule) and residues 262–274. It comprises a hydrophobic plug, which stabilizes inter-strand interactions. Therefore, oxidation of Cys374 can destabilize inter-monomer interactions. Oxidation of Cys272 might also alter the interaction of actin filaments with actin filament binding proteins (Lassing et al, 2007).

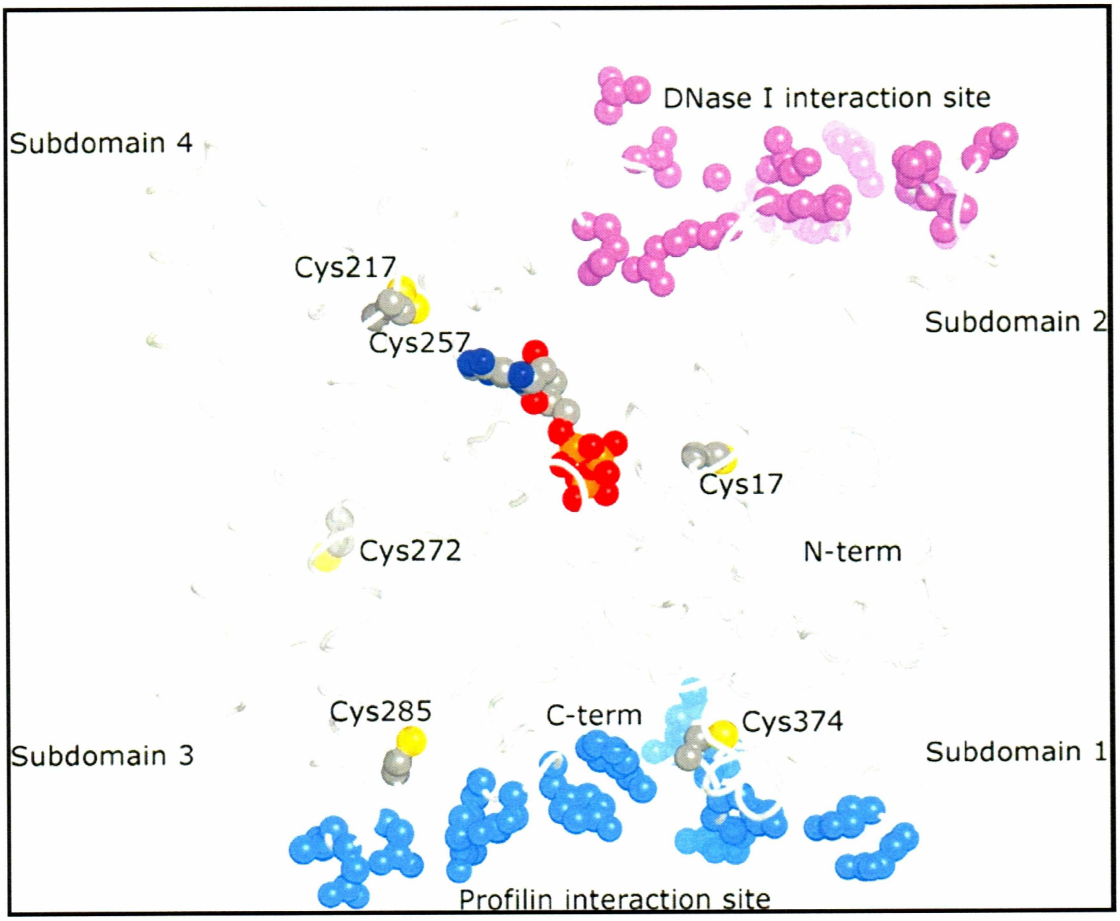

Figure 3.1 Illustration of Cysteine Residues. 6 cysteine residues in the G-actin are shown. Profilin and DNase I Interaction Sites in G-Actin are also indicated.
Source: Lassing et al, 2007, Journal of Molecular Biology, 370, 331-348.

Changes in the structure of the actin cytoskeleton involve oxidation of the reactive Cys374 to form a partially oxidized reactive sulfhydryl. This sulfhydryl then may interact

with cellular GSH to form S-thiolated actin. The mixed disulfide may be reduced, through the activities of cellular enzymes restoring the Cys374 in the protonated (SH) form (Dalle-Donne et al, 2003).

Slow thiol oxidation of monomeric actin gives rise to antiparallel dimers with a disulphide bond at Cys374. These antiparallel α-actin dimers become integrated into growing actin filaments *in vitro* and participate directly in actin filament growth (Dalle-Donne et al, 2003). Incorporated dimer sites constitute platforms for the binding of Arp2/3 to commence the formation of daughter filaments. It is possible that the increased flexibility around the disulfide bond of a filament containing an antiparallel dimer might require actin-binding proteins to stabilize the structure. Thus, Arp2/3 could enforce a particular conformation of the dimer to facilitate directed growth of the filament at a particular angle.

The susceptibility of actin to the oxidation of its reactive sulfhydryl groups has been investigated by treating purified monomeric actin with H_2O_2. H_2O_2 was found to oxidize only the reactive -SH on Cys374, leaving unaltered those at Cys10, Cys217, Cys257, and Cys285 (Dalle-Donne et al, 2003). Studies indicate that slow oxidation of G-actin produces small amounts of intermolecular disulfide-bonded actin dimers and/or oligomers. Disulfide-bonded actin dimers are incorporated into F-actin during polymerization and generate cross-links between actin filaments, enhancing the elasticity of the F-actin network.

Oxidative stress is also able to induce structural changes in the actin subdomain 2. The oxidation of Cys374 renders both chymotrypsin and subtilisin cleavage sites less accessible, resulting in a decreased protease susceptibility of the surface loop 39–51 in subdomain 2 of the actin molecule.

3.3.2 Methionine Modifications

Methionine (Met) residues represent additional potential sites of oxidative modifications. The oxidation of Methionines to MeSOX represents a common protein modification accompanying oxidative stress. Depending on the location of the modified Met residue may cause conformational changes and/or inactivation of a protein. It has been implicated in the modulation of cellular signaling processes. Actin contains 16 methionine residues, located at positions, 44, 47, 82, 119, 123, 132, 176, 190, 227, 269, 283, 299, 305, 313, 325 and 355. Some of these residues are partially exposed, whereas others are completely buried. Choramine T, an oxidizing agent, preferentially oxidizes methionine and cysteine residues (Dalle-Donne et al, 2002). Utilizing actin blocked at Cys-374, this study evaluated the effect of methionine oxidation on actin filament formation and stability. Methionines at positions 44, 47, and 355 are the most solvent-exposed methionyl residues in the actin molecule and are the most susceptible to oxidation to the sulfoxide derivative. Additional sites of the oxidative modification include Met176, Met190, Met227, and Met269.

Methionine oxidation also leads to structural alterations confirmed by decreased susceptibility to proteolysis (Dalle-Donne et al, 2002). Oxidation of Cys374 only moderately affects actin polymerization. On the other hand, oxidation of some critical methionines (those at positions 176, 190, and 269) completely inhibits actin polymerization and severely affects the stability of actin filaments, which rapidly depolymerize (Dalle-Donne et al, 2002). Oxidation of these critical methionine residues disrupts specific non-covalent interactions that normally stabilize the structure of actin filaments. It has been suggested that the formation of carbonyls within actin filaments requires a more severe oxidative insult compared to the formation of oxidized methionine (Dalle-Donne et al, 2002). Therefore, methionine oxidation could be a damaging event preceding the appearance of carbonyl groups on actin and a major cause of functional impairment of the carbonylated protein.

3.3.3 Lysine, Histidine and Arginine Modifications

Lysine, histidine and arginine are carbonylated upon exposure of actin molecules to chronic, intense oxidative stress. Actin carbonylation has been shown to inhibit F-actin formation as well as disruption of existing F-actin. Covalent intermolecular cross-linking and noncovalent aggregation of carbonylated actin have been reported as a result of HOCl mediated actin carbonylation. (Dalle-Donne et al, 2001).

3.4 Effects of Actin Oxidation

Actin oxidation affects actin dynamics and cellular processes at several levels. Reflected in cells by disappearance or disorganization of actin superstructures these effects can be broadly categorized into:

1. Redox Regulation
2. Decrease in Polymerization Rate
3. Decreased/altered Filament Stability
4. Filament Fragmentation/Disruption
5. Formation of Oligomers, Aggregation
6. Decreased/altered Affinity for Binding Proteins

ROS may promote actin polymerization by severing filaments, and/or uncapping the barbed ends of filaments required for the migratory behavior of cultured endothelial cells. ROS may promote the severing of actin filaments, the uncapping of barbed ends, or both. Whatever the mechanism for this effect might be it results in a net increase in exposure of the barbed end and an increase in the actin polymerization rate. These effects of oxidants are mediated by covalent modification of critical protein sulfhydryl residues (Moldovan et al, 2000).

Fiaschi et al, 2006 provided the first evidence of *in vivo* actin redox regulation by a physiological source of reactive oxygen species generated by integrin receptors during cell adhesion. Actin oxidation takes place via formation of a mixed disulfide bond

between cysteine 374 and glutathione. This modulation is essential for cell spreading and actin reorganization during cell adhesion.

In vivo and *in vitro* oxidation of sulfhydryl groups to sulfinic and sulfenic acids have also been reported in redox sensitive proteins, but these are terminal products leading to a permanent post-translational modification of the protein. Glultathionylation on the other hand, is a reversible protein modification that prevents permanent reorganization of the actin cytoskeleton preserves actin dynamics.

Lassing et al (2007) examined the biochemical effects of H_2O_2 induced oxidation on actin filament formation. They showed that H_2O_2 acts directly at several levels of this system. Oxidation of β/γ-actin causes a complete loss of actin polymerization that is reversed by the thioredoxin system consisting of NADPH oxidase, thioredoxin reductase and thioredoxin. In addition, oxidation of actin impedes binding with profilin. The effects of oxidation are dependent on the nucleotide state and the concentration of Ca^{2+}. Addition of ATP to oxidized ADP-actin also results in recovery of polymerization capacity. Oxidation of two cysteine residues causes a two to three fold increase in K_d for the interaction with DNase I. Exposure of actin filaments to oxidizing agents results in fragmentation of filaments rather than complete depolymerization to monomers. Structurally, oxidation results in covalent modifications of cysteines (Cys272 and Cys374) to sulfenic or sulfinic acid.

It is likely that S-thiolation, intermolecular disulfide linkages, or oxidation of critical methionyl residues of actin, affect the interactions between actin and actin-binding proteins. Oxidants selectively affect the function of actin monomer-sequestering proteins reversibly or irreversibly. Oxidative modifications of critical amino acid residues in F-actin-capping proteins or filament-severing proteins may represent a regulatory switch for initiating filament formation. In turn, oxidatively modified actin binding proteins may affect actin polymerization and/or depolymerization processes.

3.5 Actin Functional Impairment as a Result of Oxidation

In various cell types, including hepatocytes and fibroblasts, oxidative stress produces a severe disruption of the microfilament cytoskeleton characterized by the fragmentation of F-actin. Shortening of actin filaments has been associated with oxidative modifications of the sulfhydryl group of actin cysteine residues. These oligomers aggregate side-to-side into short bundles (Dalle-Donne 2001).

Human platelets, isolated hepatocytes, human fibroblasts, and other mammalian cell types exposed to the ROS-inducers 2-methyl-1, 4-naphthoquinone (menadione) and diazenedicarboxylic acid bis (N, N-dimethylamide) (diamide) exhibit a disruption of the normal organization of microfilaments with loss of protein –SH groups (Dalle-Donne et al, 2003).

One of the consequences of oxidative stress injury is a change in cell morphology and the formation of multiple surface blebs on plasma membranes (Dalle-Donne et al, 2001). Rupturing of these blebs causes loss of cellular ion gradients and the release of intracellular components, resulting in necrotic cell death. The loss of normal cell morphology has been attributed to a disruption of the actin cytoskeleton induced by the loss of Ca^{2+} homeostasis. A rise in Ca^{2+} concentration promotes the dissociation of actin microfilaments from actinin, a protein that mediates the association of microfilaments with actin-binding proteins in the plasma membrane. Ca^{2+} also activates some proteases (calpains) that cleave actin-binding proteins. This leads to the dissociation of the actin cytoskeleton from the plasma membrane and "blebbing out." The oxidation of actin is thought to contribute to the loss of normal cell morphology. The oxidation of thiol groups within actin leads to bleb formation, a decrease in G-actin levels and the formation of high-molecular weight actin aggregates. This is inhibited by thiol reducing agents. Bleb formation leads to oxidation of thiol groups, a concomitant decrease in G-actin and the formation of high molecular weight actin molecules. Moreover, bleb formation could be prevented by the addition of a thiol reducing agent (dithiothreitol or β-mercaptoethanol)

to the cell medium before treatment with menadione or diamide as an oxidizing agent (Dalle-Donne et al, 2001).

Several functions of endothelial cells such as increased cell permeability induced by mediators of inflammation and activated cell migration are associated with actin cytoskeleton reorganization (Banan et al, 2000). In many cell types, the integrity of the actin cytoskeleton is one of the earliest targets of ROS (Dalle-Donne et al, 2006). In endothelial cells, hydrogen peroxide induces the reorganization of the actin cytoskeleton, including the disappearance of membrane ruffles, disruption of cortical microfilaments, and the formation of dense stress fibers and focal adhesion complexes at the basal surface of cells (Powel et al, 2001).

Rapid and reversible actin S-thiolation (formation of disulfide adducts between actin sulfhydryls and the sulfhydryl of glutathione) is observed under oxidative stress induced by H_2O_2 or diamide (Dalle-Donne et al, 2001). Studies have revealed that exposure to both oxidants leads to the disappearance of normal stress fibers and an increase in actin polymerization in association with contraction of the cells. These morphological changes are completely reversible within minutes by the glutathione system. Glutathione-depletion on the other hand, under same conditions causes severe and irreversible contraction and detachment of cells from culture plates, leading to a decrease in cell viability.

In human intestinal cell monolayers, both H_2O_2 and HOCl enhance actin carbonylation, decrease the stable F-actin fraction and increase the monomeric G-actin fraction (Banan et al, 2000). The disruption of the actin cytoskeleton and loss of the monolayer barrier coincide with these changes.

3.6 Pathologies Associated with Actin Oxidation

Oxidant-induced cell damage is primarily mediated by the cytoskeleton, and in particular, the actin cytoskeleton. Protein carbonylation levels in β-actin and creatine kinase are significantly higher in Alzheimer's disease than in control brain extract of human subjects (Aksenov et al, 2001). Results suggest that oxidative stress-induced injury may involve the selective modification of different intracellular proteins, including key enzymes and structural proteins may lead to the neurofibrillary degeneration of neurons in the Alzheimer's diseased brain. Interestingly, in all brain regions studied in Alzheimer's disease, there is a significant decline in the activity of the enzyme peptide, methionine sulfoxide reductase, which reverses methionine sulfoxide back to methionine. A significant (80%) increase in actin carbonylation is associated with significant depression of post-ischemic contractile function.

Diamide treatment leads to disruption of actin cytoskeleton. In Friederich ataxia, a disease correlated with iron-mediated oxidative stress, actin is modified in fibroblasts (Pastore et al, 2003). Both these conditions i.e. exposure to diamide and iron mediated oxidative stress show a strong correlation between exogenous oxidative stress and high levels of actin glutathionylation and impairment of actin cytoskeletal function. Actin glutathionylation also causes disassembly of actomyosin complexes.

Actin glutathionylation is increased in patients with Friedreich's ataxia. Disulfide-linked actin oligomers in post-ischemic reperfusion in rat hearts were reported (Pastore et al, 2003). In autism, a serious neurobiological condition, neuronal migration defects and synaptic deficiencies have been suggested as the causes of hippocampal and amygdalar dysfunctions. PTEN (phosphatase Tensin homolog, mutations in this gene are found to be associated with several disorders such as autism) is linked between oxidation by H_2O_2 and Rac is implicated in the etiology of autism. It is thought to have an influence on brain development via the actin microfilament system.

3.7 Hypothesis

It is clear that actin dynamics is absolutely essential for cell survival. Actin oxidation can inhibit cellular dynamics and as a result, can prove to be lethal to cells. **I hypothesized that oxidation of actin alters kinetic parameters of actin filament dynamics.** Previously, actin polymerization has been studied in solution using pyrene-labeled actin in conjunction with UV. This modification can alter the kinetic parameters of actin filament assembly. The modified actin essentially does not remain structurally native any more. These approaches also utilize overall/average growth rates for filament formation and do not differentiate between different phases of actin polymerization; including the initial nucleation phase. To overcome these difficulties, I measured actin polymerization using Surface Plasmon Resonance (SPR). SPR permits real time analysis of kinetic parameters for addition of each monomer to the filament. This enables, for the first time, a determination of the kinetics of the nucleation phase. I measured the interaction between actin monomers during the nucleation phase and the association and dissociation kinetics of actin polymerization. These results were compared to measurements made with oxidized actin.

.

CHAPTER FOUR

Methods

4.1 Principle of Surface Plasmon Resonance

Surface plasmon resonance (SPR) allows monitoring of interactions between molecules in real time. Figure 4.1 shows components of SPR instrument by BIAcore Inc. In SPR, one interacting partner is immobilized on the surface of a sensor chip and the other interacting partner(s) is passed in a fluid stream over the surface. Binding of soluble molecules to their immobilized interaction partner on the sensor surface generates a response proportional to the bound mass. Changes as low as a few picograms or less per square millimeter can be detected using SPR. Binding events are followed in real time and a range of interaction characteristics can be determined.

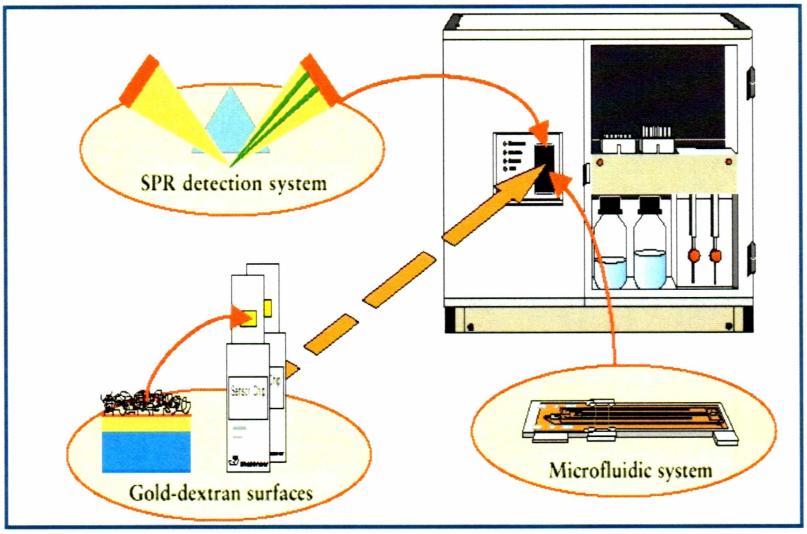

Figure 4.1 Components of SPR. Gold-dextran Surface, Microfluidic System and Detection System are major components of SPR instrument. (Source: Biacore Instrument Handbook)

SPR can address

1. Specificity of biomolecular interactions
2. Kinetics (association and dissociation rates) and affinity of interactions by analyzing the time curve and amplitude of binding in terms of molecular interaction models.

4.2 SPR Terminology:

- The interaction partner attached to the sensor surface is called the ligand. The term is consistent with the terminology used in affinity chromatography and does not imply that the surface-attached molecule is a ligand for a cellular receptor.
- The analyte is the interaction partner that is passed over the immobilized ligand in solution.
- Analysis is performed by injecting the sample in a controlled fashion. The sample is carried in a continuous flow of buffer called the running buffer.
- Regeneration is the process of removing the bound analyte from the surface after an analysis without damaging the ligand.
- Response is measured in resonance units (RU). The response is directly proportional to the concentration of biomolecules on the surface. 1 RU response corresponds to binding of 1 ng of molecule on the sensor surface.
- A sensogram is a plot of response versus time showing the progress of interaction. This curve is displayed on the computer screen during the course of analysis.

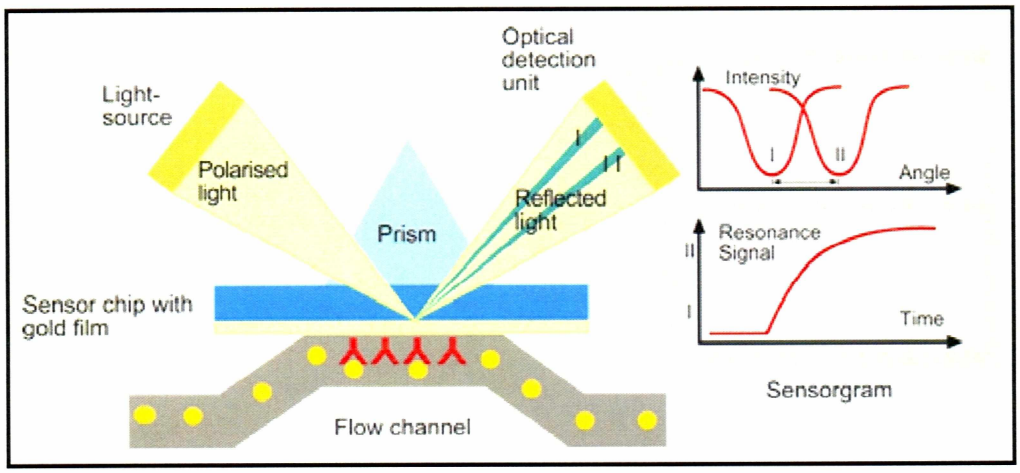

Figure 4.2 SPR Detection Principle. (Source: Biacore Application Handbook)

4.3 SPR Phenomenon

SPR is a phenomenon that occurs in thin conducting films at an interface between media with different refractive indices. Figure 4.2 shows how SPR phenomenon is employed in this method. In this technique, the two media are the glass of the sensor chip and the sample solution. The conducting film is a thin layer of gold on the sensor chip surface. Under conditions of total internal reflection, light incident on the reflecting interface emits an electric field intensity called the Evanescent wave field, across the interface into the media with the lower refractive index, without losing net energy. The amplitude of the Evanescent wave field decreases exponentially with distance from the surface and the effective penetration depth in terms of the sensitivity to refractive index is about 20% of the wavelength of the incident light. Because the Evanescent wave field penetrates the solution, conditions for this resonance effect are very sensitive to the refractive index of the solution within the effective penetration depth of the Evanescent wave field. Changes in solute concentration at the surface of the sensor chip cause changes in the SPR conditions. The penetration depth of the Evanescent wave determines the thickness of the solution layer where refractive index changes close to the surface affect the SPR signal. To achieve total internal reflection of the light at the interface between the sensor chip and the solution, the glass side of the chip is pressed against a semi cylindrical glass

prism using a silicon opto-interace. Light from a light-emitting diode (wavelength 800nm) is focused in a wedge on to the sensor surface covering fixed range of incident and reflected angles. The effective penetration depth of the Evanescent wave under these conditions is on the order of 150 nm. Gold combines favorable SPR characteristics with stability and inertness in biomolecular interaction contexts. Coating on gold layer provides a means of attaching ligand and an environment where the interaction being studied can occur. The gold layer and the surface coating are stable under a wide range of conditions. Once the ligand has been immobilized, the resistance of the sensor surface to various agents and conditions is determined by the properties of the attached ligand.

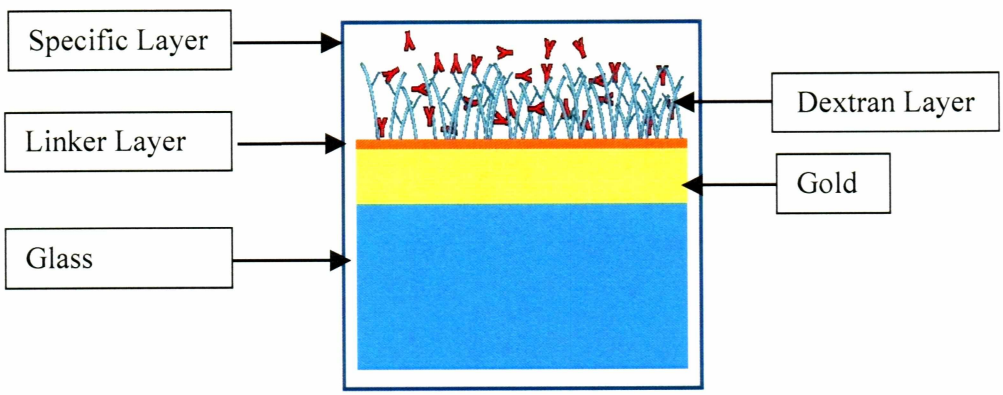

Figure 4.3 Gold-dextran Surface of Sensor Chip CM5 (Source: Biacore Instrument Handbook)

4.4 Sensor Surface

The Biacore CM5 chip was primarily used for the work described in this thesis. Figure 4.3 shows the components of the chip. This chip is composed of a carboxy-methylated dextran matrix coated onto a gold surface. The Dextran matrix is flexible allowing free movement of the attached ligand within the surface layer. It extends about 100 nm from the gold surface under physiological buffer conditions. The SPR angle is determined at a frequency of 160 Hz (measurement per second). It is then averaged by a microprocessor

in the instrument and transmitted to the control software at rates up to 10Hz. When multiple flow cells are used, buffer flows through the cells in series. The dead volume between the flow cells is 0.3 µl. At a flow rate of 20 ul/min, the delay between the flow cells is about 1 s corresponding to one data point at medium data collection rate.

4.5 Scouting and Immobilization

Electrostatic attraction of the ligand to the surface is the main mechanism for immobilization of ligands. The carboxymethylated surface of the sensor chip carries a net negative charge at pH values about 3.5. Hence, the effective preconcentration of ligand on the surface is achieved in a buffer with of a pH higher then 3.5 and lower than the isoelectric point of the ligand. Retention of the functional interaction between the ligand and anylate is a primary requirement for immobilized ligands. Ligand molecules bound to the matrix are freely accessible in three dimensions and are expected to behave the same as in aqueous solution. However, biological activity of the ligand may be adversely affected by the coupling reaction. Steric restrictions may arise both with large ligands and analytes. There is also a decrease in the entropy of the interaction due to the immobilization of one binding partner. This could create a slight increase in the affinity of the ligand for the bound molecule.

4.6 Amine Coupling

The experiments described here primarily used amine coupling for immobilization of ligand. Amine coupling utilizes amino groups on the surface of the ligand for immobilization. The site of ligand immobilization and its orientation cannot be determined because the chip potentially interacts with multiple amino groups the ligand. This results in a heterogenous population of ligand immobilized in multiple orientations on the sensor surface. A subset of these ligands may be unable to bind analyte due to steric effects.

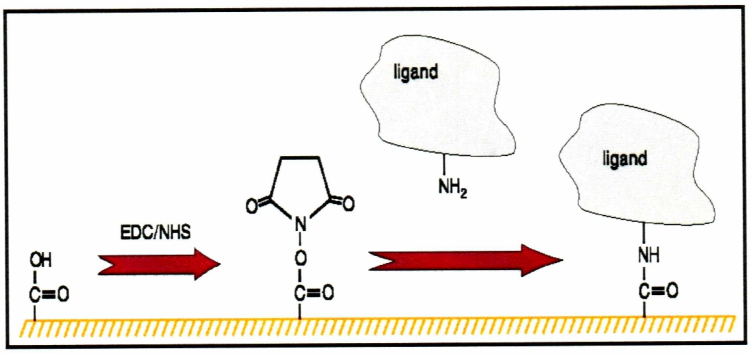

Figure 4.4 Standard Amine Coupling Immobilization Method (Source: Biacore Instrument Handbook)

Table 4.1 Reagents for Standard Amine Coupling Method

NHS	1 M N-hydroxysuccinimide in water
EDC	0.4 M 1-ethyl-3-(3-dimethylaminopropyl)-carbodiimide in water
Ethanolamine	1M ethanolamine-HCl pH 8.5
Ligand	20-50 μg/ml in immobilization buffer

The dextran matrix on the sensor chip is first activated with a mixture of 1-ethyl-3-(3-dimethylaminopropyl) carbodiimide (EDC) and N-hydroxysuccinimide (NHS) to form reactive succinimide esters. The ligand is then passed over the surface and the esters react spontaneously with amino groups or other nucleophilic groups, to covalently bind the ligand to the dextran. Any remaining active esters on the surface are deactivated by ethanolamine after injecting the ligand (see Figure 4.4). Washing with a high ionic strength buffer removes any non-covalently bound ligand.

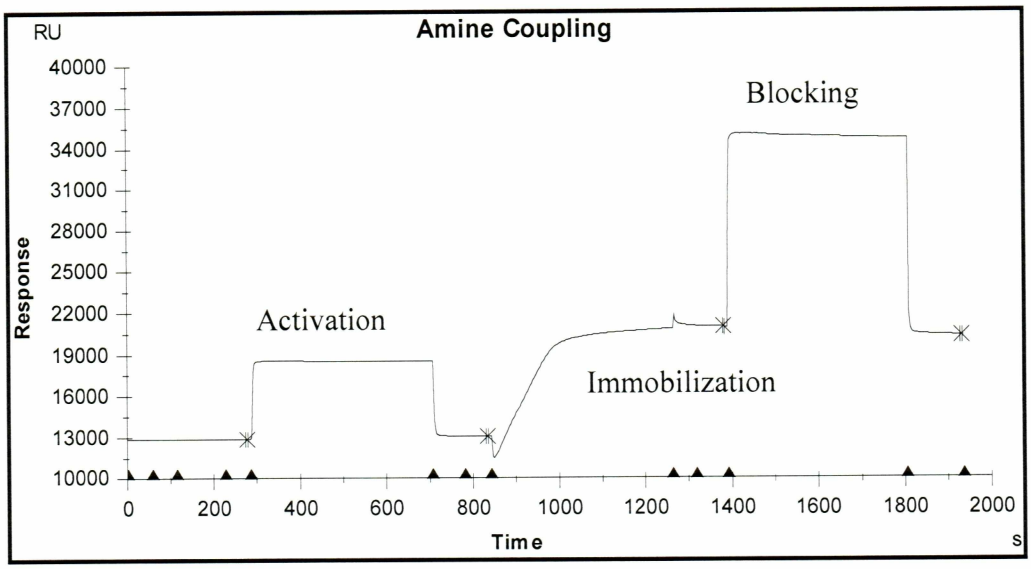

Figure 4.5 Standard Sensogram for Immobilization by Amine Coupling. The first part of sensogram shows the activation of surface esters by NHS/EDC followed by the attachment of the protein on activated surface. The third part of the sensogram represents the blocking of remaining esters by ethanolamine in order to avoid any nonspecific binding.

4.7 Immobilization Levels:

The binding capacity of the surface depends on the levels of immobilized ligand present on the surface. The maximum response (R_{max}) describes the binding capacity of the surface at saturation. The theoretical value of R_{max} can be calculated using the formula below.

$$R_{\max} = \frac{A}{L} \times I \times S \qquad \text{Equation 1}$$

Where A and L are the molecular weight of the analyte and ligand respectively, I is the amount of ligand immobilized and S is the stoichiometric ratio of analyte to ligand. The theoretically calculated R_{max} is often higher than the experimentally derived value for the same interaction. There can be many potential reasons for this discrepancy. The ligand may not be in the proper orientation or conformation, immobilization may have altered

the binding characteristics of the ligand or steric hindrance may limit the anylate/ligand interaction.

4.8 Kinetic Measurements

When the analyte is injected under favorable buffer conditions, the resulting sensogram can be divided into three sequential phases (Figure 4.6).

- Association of analyte with ligand during sample injection
- Equilibrium or steady state. (The rate of analyte binding is balanced by rate of dissociation from the complex during the sample injection).
- Dissociation of analyte from the surface during buffer flow.

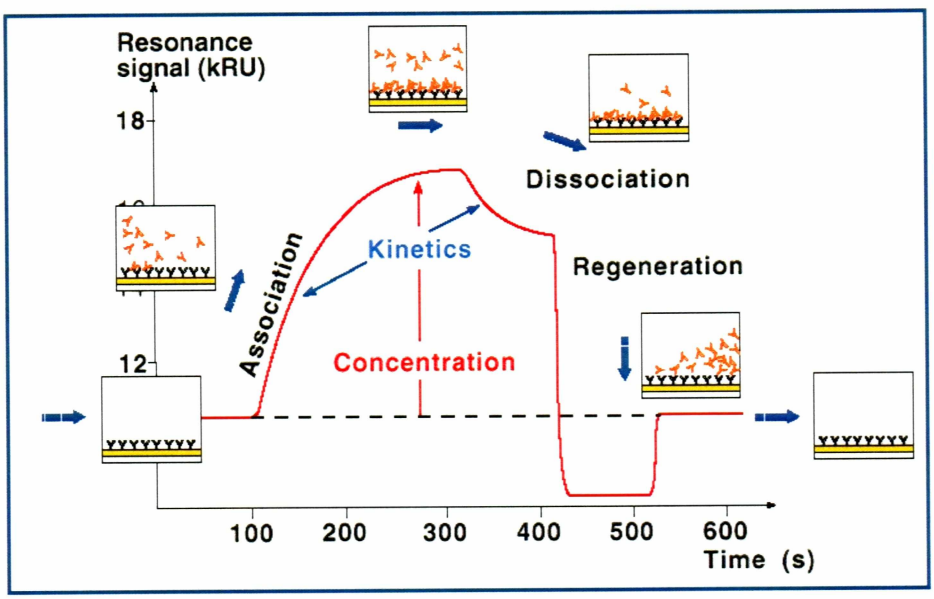

Figure 4.6 Standard Sensogram of a Kinetic Experiment. (Source: Biacore Application Handbook). The sensogram starts with a stable baseline. The binding response increases binding of two molecules (one immobilized on the surface of the sensor chip and other passed in solution over the sensor surface). The signal goes down as the two molecules dissociate. The trace is completed with clean up of the surface to prepare for the next cycle.

The association and dissociation phases provide information on the kinetics of the interaction i.e. the rates of complex formation and dissociation. The equilibrium phase provides information on the affinity of the analyte-ligand interaction.

Extracting rate constants from the sensogram is carried out in following steps.

1. Measurement of the binding curves
2. Deciding on a model to describe the interaction
3. Fitting the curve to a mathematical rate equation describing the model
4. Obtaining values for the constants k_a, k_d, R_{max}
5. Assessment of the fit
6. Acceptable statistics e.g. chi^2 – curve fidelity
7. Biological and experimental relevance of the calculated parameters

A homogeneous 1:1 interaction on the sensor chip surface may be described by the equation:

$$[A] + [B] \rightleftharpoons [AB]$$

For this model:

Association rate: $\frac{[AB]}{dt} = \text{ka} \cdot [A] \cdot [B]$

Dissociation rate: $-\frac{[A][B]}{dt} = kd \cdot [AB]$

At equilibrium: Association = Dissociation

$$ka \cdot [A] \cdot [B] = kd \cdot [AB]$$

The equilibrium constant:

$$\text{Keq} = \frac{[AB]}{[A] \cdot [B]} = \frac{ka}{kd}$$

4.9 Equilibrium and Kinetics with SPR

In this method:

$[A] + [B] \rightleftharpoons [AB]$

$K_{eq} = [AB]/ [A] [B]$

[A] = Protein immobilized on chip (known)

[B] = Protein ran as sample (known)

[AB] = Resonance units measured

A is the analyte in the solution. The free concentration of the analyte is maintained constant by the flow system. AB is the complex formed with the two binding partners and concentration of this complex is measured directly as Response in Resonance unit. B is the ligand on the surface of the sensor chip. The total concentration of B can be expressed in RU as maximum binding capacity R_{max}. Hence the free concentration becomes R_{max}-R.

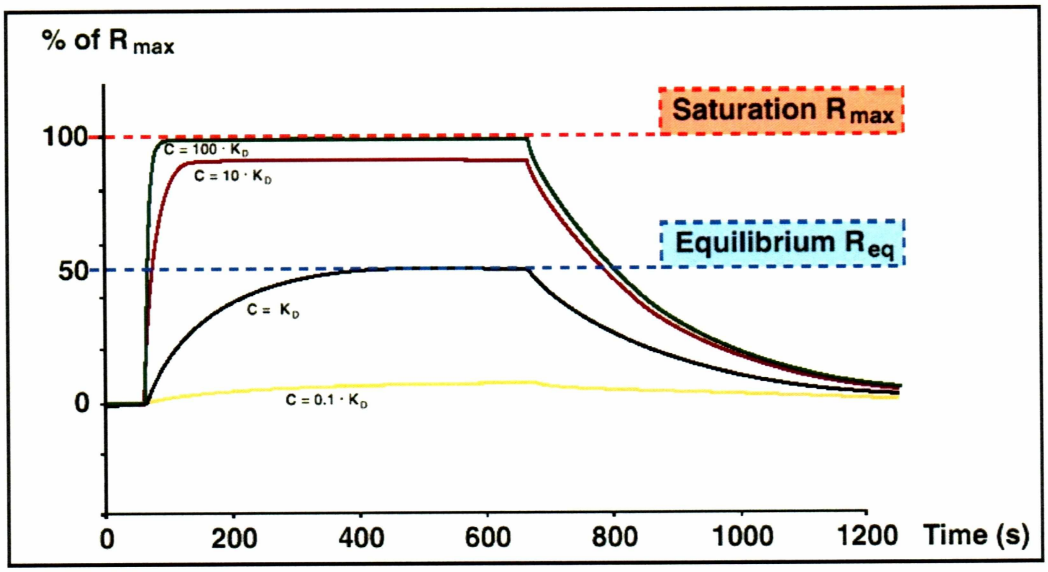

Figure 4.7 Extraction of Information from the Sensogram (Source: Biacore Application Handbook)

As shown in figure 4.7, a dilution series of antibody generates a response proportional to the concentration. The first part of the curve, where the binding response rises above the baseline, represents association, or the binding of the two molecules. The second phase of each curve is called dissociation phase, where the two molecules dissociate from each other. Dissociation starts at the end of the injection of the sample on the sensor surface. The binding curves are then double referenced i.e. each curve is subtracted from a control response on the reference surface on the same sensor chip. Each curve is also subtracted from a control using buffer injected over the immobilized surface. This is the best way to control for any effects of buffer on the binding curves.

To quantify the binding affinity of any two interacting molecules, the molecular weight of the two molecules, the concentration of the analyte injected and the amount of immobilized ligand must be known.

$$R_{\max} = \frac{A}{L} \times I \times S$$

In any binding experiment, if one molecule of ligand binds to one molecule of analyte, it generates a response of one resonance unit if the molecular weight of the two molecules is same. For example, the molecular weight of actin is 43000 Da. and the molecular weight of the antibody is 150 Dalton, which is about three times the molecular weight of the ligand. When one molecule of antibody binds to one molecule of actin on the chip surface, it generates a response of three resonance units.

CHAPTER FIVE

Interaction of Actin with Monoclonal Anti-Actin Antibody and DNase I

5.1 Interaction of Actin with Monoclonal Anti-actin Antibody using SPR

Our primary aim was to confirm that SPR can be used to study protein–protein interactions with actin as an interaction partner.

5.1.1 Reagents

Lyophilized rabbit skeletal muscle actin was purchased (Cytoskeleton Inc.). After reconstitution in water, the actin solution contained 2mM ATP, 0.2 mM $CaCl_2$, 1% dextran, 5mM Tris-Cl (pH 7.4). Under these buffer conditions (low ionic strength, no potassium), actin remains in its monomeric ATP-bound globular conformation (G-actin buffer). Since Tris containing buffers are known to interfere with the optical detection of SPR, Tris was removed from purchased actin using a spin column (5000 Dalton cut off). Filtered actin was then dissolved in modified SPR-G-actin buffer (HBS-EP, 5mM ATP, 0.2 mM $CaCl_2$). This also removed dextran and sodium azide, which can increase non-specific binding. Rebuffered actin was stored at –20°C. All other chemicals were purchased from Sigma-Aldrich unless otherwise noted. CM5 sensor chips and HBS-EP buffer were purchased from BIAcore Inc. HBS-EP buffer consists of 0.15 M NaCl, 10 mM HEPES, pH 7.4, 3 mM EGTA and 0.005% polysorbate 20(v/v). All buffers were filtered and equilibrated to room temperature for two hours before use. A monoclonal mouse anti-chicken actin antibody (isotype IgG1 kappa) was obtained from Chemicon Inc. (MAB1501). The antibody binds to an epitope within the highly conserved N-terminal region of actin (amino acids 50-70) present in all six actin isoforms. Previous solution studies have determined the affinity constant at a range of 3-15 x 10^8 M^{-1}.

5.1.2 Surface Preparation

Preconcentration scouting is the initial step of any sensor chip surface preparation. This step is necessary to find suitable pH conditions and optimum ligand concentrations for immobilization. A 10 mM Na acetate buffers (NaAc) with pH ranging from 5.5 to 4.0 were tested to find out the optimal pH to immobilize actin (Fig 5.1a). Another representation of the scouting procedure (Fig 5.1b) shows how the electrostatic attraction of actin for the sensor surface varies as a function of pH. NaAc buffer pH 4.0 exhibited the highest response of actin interaction with the sensor chip surface or the maximum electrostatic attraction of the ligand actin for the particular sensor surface.

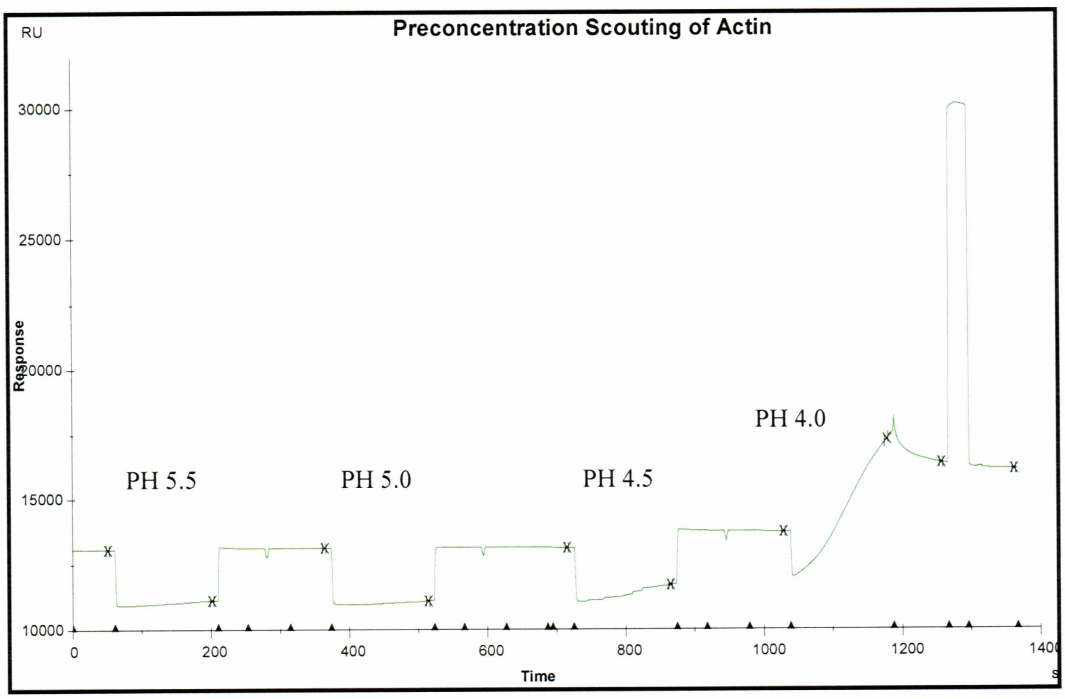

Figure 5.1a Preconcentration Scouting of Actin. 20 μg/ml actin diluted in 10 mM Na acetate buffer with pH 5.5, 5.0, 4.5, and 4.0 are injected. Increases in RU is indicative of the degree of attraction of actin to the sensor chip surface. Buffer pH influences density of exposed amine groups on the surface of the protein. At pH 5.5 there is no rise in resonance signal as compared to pH 4.0.

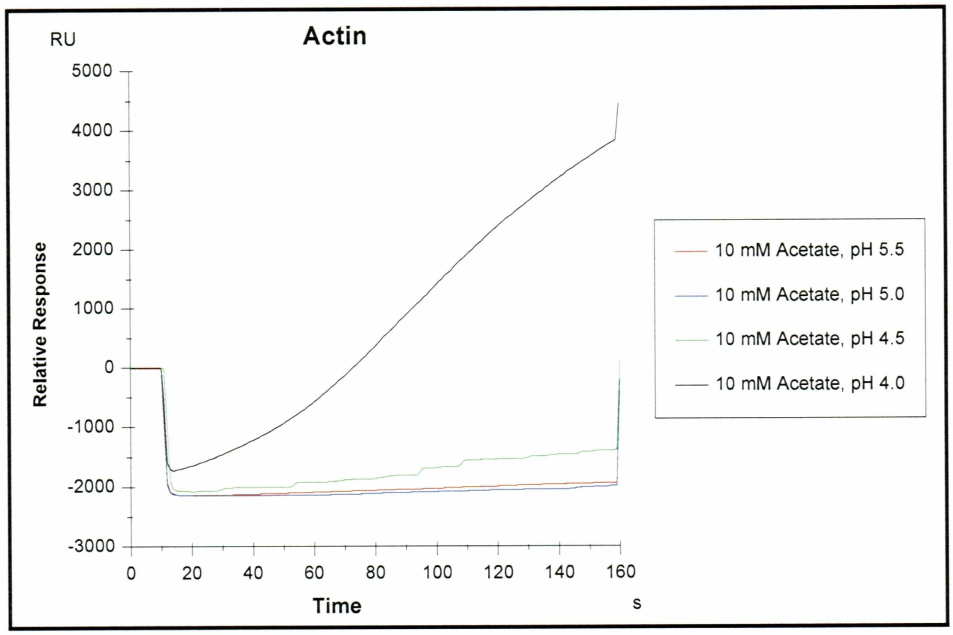

Figure 5.1b Preconcentration Scouting of Actin. Another representation of the same data set shown in figure 5.1a. Actin in Na acetate buffer pH 4.0 shows the highest response when the relative responses in different pH buffers are plotted versus time.

Several actin concentrations (2 μg/ml-100 μg/ml) were tested to achieve desired immobilization level with actin on the chip surface. HBS-EP buffer was used as the elution buffer. The optimum actin concentration was determined to be 20 μg/ml (data not shown).

5.1.3 Immobilization

Flow cell two on the sensor chip was used to immobilize actin. Actin was immobilized using the standard amine-coupling method (as described in Chapter FOUR) on a dextran surface of the second flow cell sensor chip (CM5 Biacore).

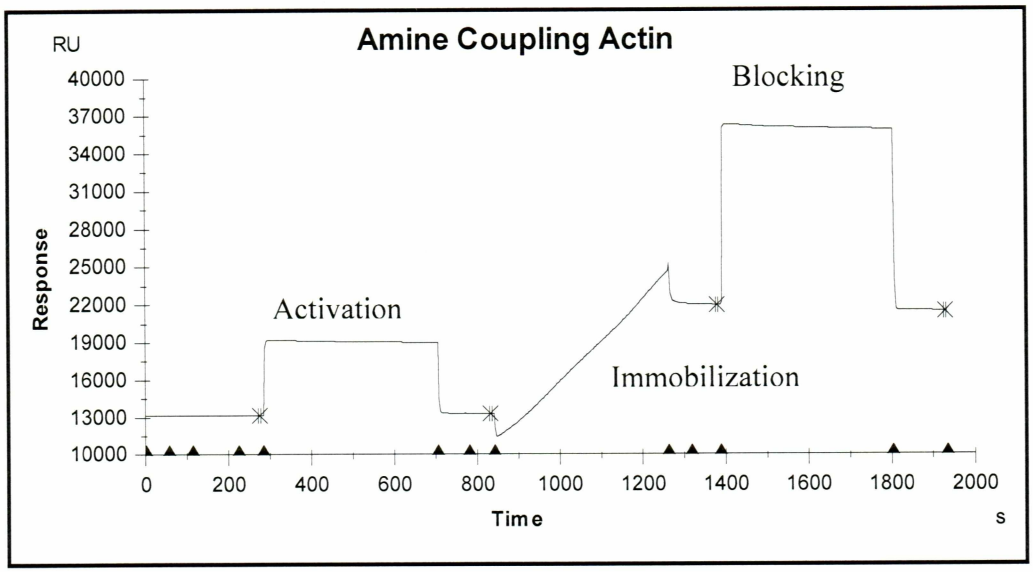

Figure 5.2 Immobilization of Actin on Sensor Chip. The graph shows activation of the dextran surface, immobilization of actin and blocking of remaining esters on the activated surface.

A response of 8300 RU was obtained, which is equivalent to $12x10^{10}$ molecules of bound actin per cm^2 area of chip surface. A reference surface was created in the first flow cell of the same sensor chip using 1 M ethanolamine as a blocking agent. Importantly, the active actin surface may cover only a fraction of the actual immobilized surface. A significant number of immobilized molecules could be in an unfavorable orientation that inhibits binding with the analyte. As different binding partners bind to actin at different site on the molecule, the percentage of the chip surface containing bound actin varies according to the specific binding partner or analyte. The percentage of active surface can be determined by injecting varying concentrations of analyte and comparing it to the theoretical maximum binding response. The theoretical maximum binding response R_{max} can be calculated by the equation:

$$R_{\max} = \frac{A}{L} \times I \times S$$

Where A is the molecular weight of the analyte, L is the molecular weight of the ligand immobilized, I is the amount of ligand immobilized (in RU) and S is the stoichiometry of the binding interaction or no of binding sites on the ligand for analyte. The active surface on this particular surface with actin was found to be about 3 % of the immobilized amount.

5.1.4 Kinetic Experiment

The monoclonal antibody was diluted with HBS-EP buffer to concentrations ranging from 150 nM to 0.1 nM (at least 10 times above and below expected affinity constant). HBS-EP was also used as the running buffer for the experiment (25°C). The binding of the antibody to immobilized actin was measured by SPR in the Biacore2000 instrument using two parallel flow cells: one containing immobilized actin (test cell) and one containing no immobilized actin (reference cell). Following a 1 min stable base line reading with running buffer only, different antibody concentrations were injected for 2 min each (association phase) at a rate of 20 µl/min. The immobilized actin on the sensor chip surface was regenerated to remove bound antibody using 10 mM glycine-HCl (pH 3.5) for 0.5 min at a rate of 20 µl/min prior to a subsequent injection of another antibody concentration. Regeneration causes dissociation of any residual analyte, i.e. antibody, on the surface without affecting the ligand on the sensor surface. As a control, identical mock solutions (i.e., devoid of antibody) were applied before introducing solutions containing the analyte (i.e., containing antibody at the given concentration).

5.1.5 Results and Discussion

The data in figure 5.3a demonstrates the direct and selective binding of the monoclonal anti-actin antibody to G-actin in a dose dependent manner displaying saturation kinetics. All real time SPR traces (raw data) were normalized for quantitative analysis. First the regeneration segment of each trace was removed (Fig 5.3b). Second, sample injection into the reference cell was subtracted from all data traces generated in the test cell.

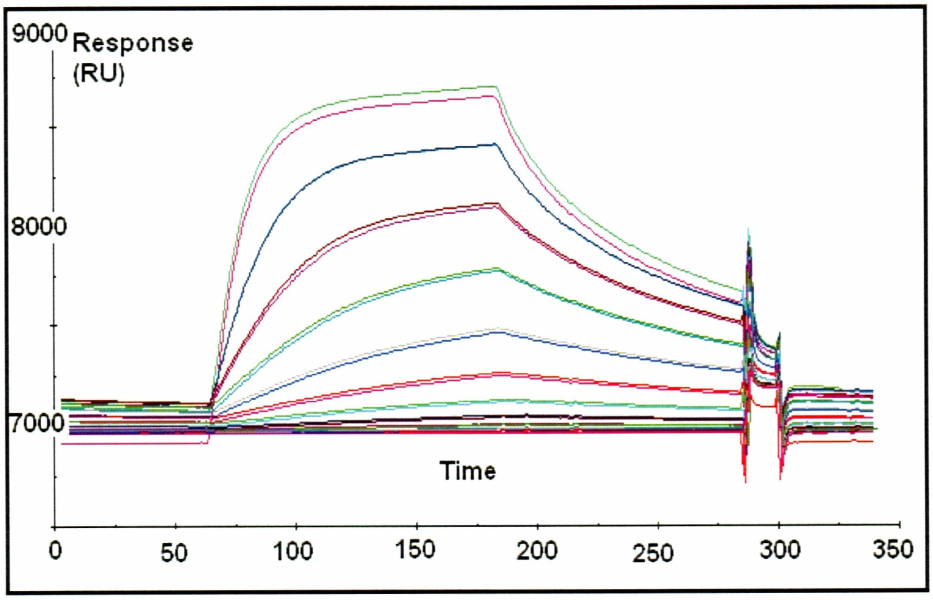

Figure 5.3a Raw Data of Actin-anti-Actin Antibody Interaction

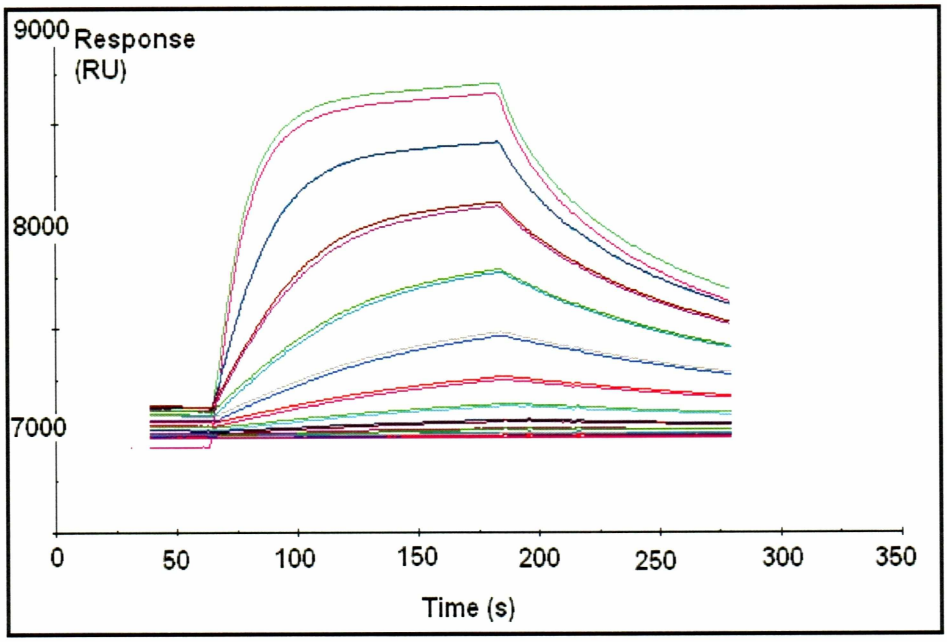

Figure 5.3b Data after Editing Regeneration Step.

As a result of normalization, association and dissociation phases can be assigned to each trace. The range of those data points is selected for each antibody concentration injected into the test and the reference cell. Then, the concentration of each antibody sample and the corresponding maximum binding response are put into the following equation to calculate real time association and dissociation rate constants.

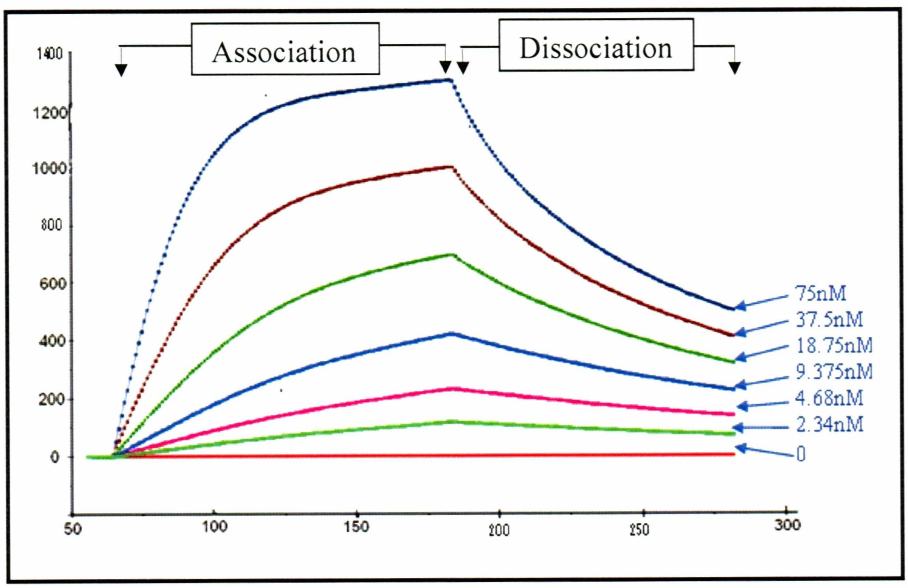

Figure 5.3c Normalized Sensogram for Interaction of Actin with Monoclonal Anti-actin Antibody. Graph shows the part of traces considered for real time association and dissociation rate constants.

The change in resonance signal is extracted as a function of time with [A] (immobilized actin) being constant and [B] (antibody concentration) a variable. Maximum increase in RU for each antibody concentration is determined and divided by the time period required to reach maximum response (RU per time unit). The change in RU per time unit is then plotted against the corresponding antibody concentration. According to the equation below, the linear relation of the plot is used to calculate association and dissociation rate constants from the slope. Since we tested every antibody concentration six times, six linear functions are established resulting in six values for each rate constant and providing a standard deviation.

Association rate: $\frac{[AB]}{dt} = ka \cdot [A] \cdot [B]$

Dissociation rate: $-\frac{[A][B]}{dt} = kd \cdot [AB]$

Where,

[A] = Actin immobilized on chip

[B] = Concentration of antibody sample

[AB] = Resonance units

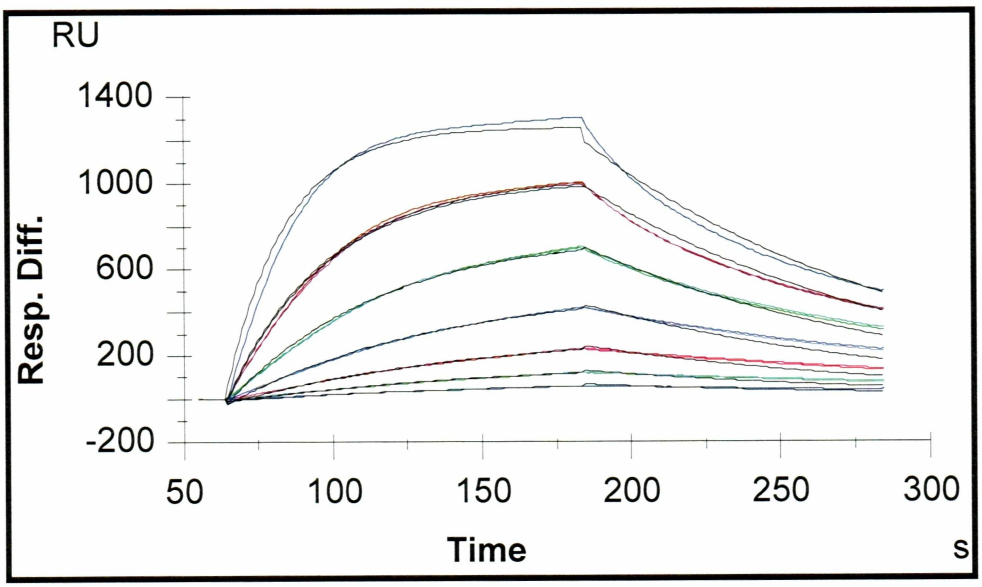

Figure 5.3d Data for Interaction of Actin with Monoclonal Anti-actin Antibody Fitted to 1:1 Binding Model.

As shown in figure 5.3d, curves were fit to a mathematical rate equation describing a 1:1 binding model to test how reliable the calculated kinetic parameters were. This in turn can be used to determine the affinity constant for the interaction between actin with its monoclonal antibody. The standard deviation for each value is calculated as the root mean square deviation. The average association rate (k_a) was

calculated as $5.49x10^5$ $M^{-1}sec^{-1}$ (n=6, SD +/- 0.012). While the average dissociation rate (k_d) was calculated as $8.98x10^{-3}$ sec^{-1} (n=6, SD +/- 0.008). The theoretical maximum response was calculated as 1460 RU, which predicts the maximum binding response at saturating concentration of the antibody. This information can be used to simulated theoretical curves, which are then compared with the experimental traces to test curve fidelity. The chi^2 value for this fit was between 2.69-3.2. The lower chi2 value the smaller is the deviation between simulated curves and experimental traces. The apparent affinity constant for the antibody–actin interaction was calculated as 16 nM. The affinity for this particular antibody was previously determined at 30-150 nM.

5.1.6 Conclusions

Conclusively, our experiments demonstrated that some fraction of actin monomers bound to the sensor chip surface remain in their native conformation thus capable of interaction with the antibody. Moreover, our data provides kinetic parameters in accordance with measurements obtained with other technologies. However, SPR analysis extracts kinetic parameters from real time measurement of interactions.

5.2 Actin-DNase I interaction Using SPR

DNase I is a deoxynuclease enzyme. It binds to actin to form a highly stable catalytically inactive1: 1 complex. The affinity of this interaction is known to be 5-10 μM (Vidali et al, 2001). The specificity of this interaction has been used to affinity purifiy actin from cell lysates, and to study thermal denaturation of monomeric actin and *in vitro* folding of actin by chaperonins. The aim for this particular set of experiments is to show that interaction of actin with it binding partner can be studied with SPR.

5.2.1 Reagents

Lyophilized bovine pancreatic DNase I grade II was purchased from Roche Applied Inc (stored at -20° C).

5.2.2 Kinetic Experiment

Actin was immobilized by amine coupling method. Sensor surface preparation and the kinetic experiments were carried out as described for actin-antibody interaction (5.1). 50 µM –0.5 µM DNase I was used for kinetic characterization of the interaction of actin with DNase I. For efficient binding to actin, DNase I requires a divalent cation such as Mg^{2+}. Thus 2 mM $MgCl_2$ was added to HBS-EP (DNase I buffer). DNase I was diluted in running buffer (2 mM $MgCl_2$ added to HBS-EP) and injected at a flow rate of 30µl/min for 2 min. 10 mM Glycine-HCl (pH 3.0) was used as a regeneration solution. DNase I was allowed to dissociate from the chip for 10 min before the injection of the regeneration solution. The baseline was allowed to stabilize for 10 min after each regeneration cycle.

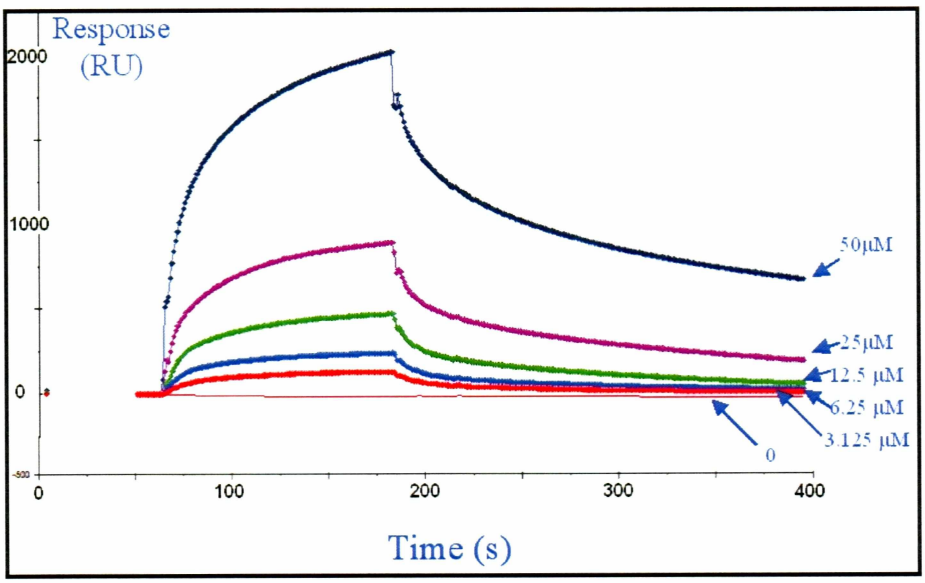

Figure 5.4 Concentration-dependent Binding of DNase to Actin. The concentration of DNase I used for each trace is shown on right hand side. DNase I was passed over immobilized actin on the sensor surface in buffer condition favouring binding of the two proteins. The regeneration step is cut out and the traces are double referenced.

5.2.3 Results and Discussion

We found that DNase I binds actin in a dose dependent manner. The data traces were analyzed using a 1:1 binding model similar to analysis of actin-antibody interaction traces (see 5.1). The average associate rate constant (k_a) was calculated as $7.7x10^2$ $M^{-1}sec^{-1}$ (n=6, SD +/-0.006) while the dissociation rate constant (k_d) was calculated as $3.19x10^{-3}$ sec^{-1} (n=3, SD +/-0.011). The theoretical maximum response was calculated as 342 RU resulting in the chi^2 value of 1.9-2.7. This value represented an excellent fit for a 1:1 binding interaction. The average calculated affinity (n=3, SD +/-0.003) was 4.2 μM. The known affinity published by Vidali et al (Vidali et al, 2001) is 5-7 μM.

5.2.4 Conclusions:

Our results indicate that actin can be immobilized without altering its binding properties. The binding of DNase I to actin indicates that DNase is functional and not denatured. This will allow us verify the integrity of each actin-coated chip prior to kinetic analysis. If actin is denatured, it will not bind to DNase I or the actin antibody. The binding site on G-actin molecule for DNase I lie on the pointed end of the molecule. As DNase I is passed on the actin surface in solution phase, it is dispersed in various orientations and there is less possibility of not having DNase I in correct orientation in order to bind to actin. Actin on the other hand amine-coupled to the sensor surface. As DNase binding can be revealed it is obvious that the binding site that is the pointed end of significant number of immobilized actin molecules is not blocked by coupling procedure. This is to be noted because antibody can bind to denatured protein but DNase I need a functional protein on the sensor surface in order to show detectable binding. Depending on where the binding site lays the immobilized surface can show different activity towards different binding partners.

CHAPTER SIX

Interaction of Actin with ATP

6.1 Introduction

Binding of nucleotide diphosphate or triphosphate has vast implications on actin dynamics. The binding site for nucleotide di/triphosphates is located between the two major domains of the actin monomer forming an ATP-binding cleft. The specific role of ATP and actin's ATPase activity impacts the actin polymerization process. ATP hydrolysis alters the stability of actin polymers rather than its assembly kinetics. The Actin-ADP complex can also form polymers but the resulting filaments are less stable and prone to depolymerization. *In vivo* Profilin is an important actin regulatory protein that facilitates the exchange of ADP with ATP, thus favoring actin polymerization and stability of F-actin.

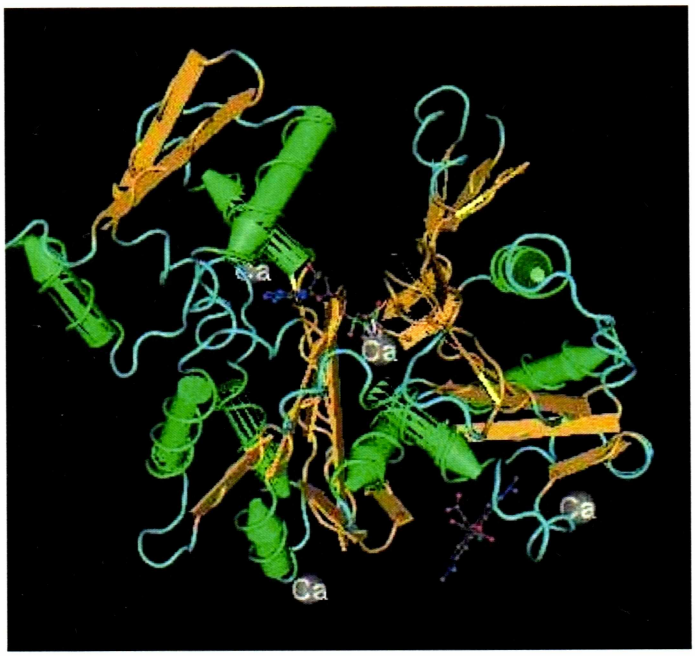

Figure 6.1 Three Dimensional Structure of G-Actin-ATP Complex. NCBI PDB structure 1NWK shows ATP and calcium binding site on G-actin molecule.

Therefore, the rates of association and dissociation of actin from each end of F-actin are dependent on the nucleotide composition of the terminal subunits (figure 6.1) Pollard (Pollard, 1986) used electron microscopy to measure association and dissociation rates of actin in its ATP versus ADP-bound state for the fast-growing and slow-growing ends.

Table 6.1 Rate Constants of Interaction of Actin with ATP and ADP.

	ATP-actin	ATP-actin	ADP-actin	ADP-actin
	Fast-growing	Fast-growing	Slow-growing	Slow-growing
k_+ ($\mu m^{-1}s^{-1}$)	11.6	1.3	3.8	0.16
k_- (s^{-1})	1.4	0.8	7.2	0.27

(Data taken from Pollard, 1986)

6.2 Kinetic Experiment

Actin was immobilized on CM5 sensor chips using the standard amine coupling method (see chapter 5.1). Since binding of divalent cation especially Mg^{2+} facilitates binding of ATP to G-actin, $MgCl_2$ was included in the HBS-EP buffer. A freshly prepared ATP stock solution was diluted into HBS-EP containing 2 mM $MgCl_2$ to concentrations ranging from 6 mM to 0.75 mM. HBS-EP/$MgCl_2$ devoid of any ATP was used as the running buffer for the kinetic experiments carried out at 25° C. The binding of ATP to immobilized actin was measured in parallel flow cells; one with actin immobilized, the other with no immobilized actin as a reference cell. Following baseline stabilization with running buffer, increasing ATP concentrations were injected for 2 min (association phase) at a rate of 75 µl/min. A wait period of 3 min was added prior to regeneration in order to monitor the native self-dissociation rate in the absence of the regeneration buffer. The baseline level was unaltered and stable after regeneration. As a control, identical

mock solutions (i.e., devoid of ATP) were applied before introducing solutions containing the analyte (i.e., containing ATP at the given concentration).

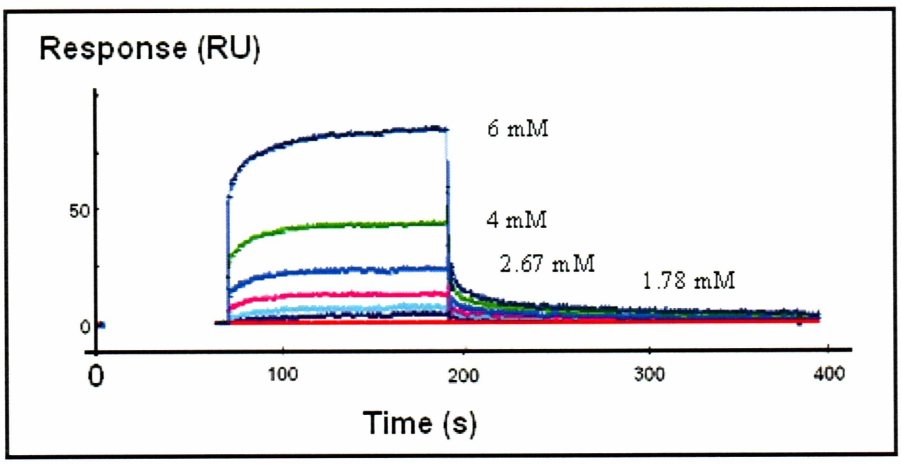

Figure 6.2 Sensogram of Binding Interaction of Actin and ATP. ATP exhibits rapid association (k_a= 8.2 $\mu M^{-1}sec^{-1}$) and dissociation (k_d=0.97 sec^{-1}) with immobilized actin. Freshly prepared ATP solution was passed over immobilized actin on sensor surface using different concentrations as indicated. The association of ATP with actin was monitored at a flow rate of 75 µl/min for 2 min and dissociation phase was monitored for 3 minutes after the end of injection.

6.3 Results and Discussion

ATP was found to bind to immobilized actin on the sensor chip in a concentration dependent manner. As discussed in chapter 5.1, actin-ATP binding curves were normalized. Actin binds ATP to form a 1:1 binding complex. Hence the data was analyzed using a 1:1 binding model. The region of the normalized sensogram between the ATP injection point and 3 min after the end of the injection was used for analysis of binding kinetics. The average association rate constant (k_a) was determined as 8.2 $\mu M^{-1}sec^{-1}$/M/s (n=6, +/-0.008) while the average dissociation rate constant (k_d) was calculated as 0.97/s (n=6, +/-0.012). The theoretical maximum response was found to be 134 RU resulting in a chi^2 value of 1.2-1.5. The overall ATP affinity of actin was calculated as 112 nM.

6.4 Conclusions:

These findings confirm that actin immobilized on the surface of the sensor chip is functional and capable of binding with ATP. Thus actin can be immobilized without altering its binding interactions with ATP and likely other interaction partners. As SPR can detect binding of ATP, which is 551 Dalton, it can be used to study actin-small molecule interaction. Pollard and Cooper, 1986 have reported about 6-10 μM affinity. The experimental affinity actually seems about ten fold higher than reported. Our data suggests that SPR might actually represent a system closer to the actual cellular environment. A nanomolar range affinity of actin for ATP would allow fast loading of G-actin with ATP whenever needed to form filament or other structures. Fast actin-ATP kinetics facilitates overall actin dynamics in cell.

CHAPTER SEVEN

Actin-actin Interaction

7.1 Actin-Actin Interaction under Reducing Conditions

As discussed in chapter one, G-actin monomers containing both ATP and Ca^{2+} will form actin filaments in a polymerization reaction. Although an actin filament assembles predominantly at the fast-growing end as a result of the low critical concentration for that particular end, initially slow-growing ends will also undergo polymerization until the free actin monomer concentration drops below the critical concentration for slow growing ends. As a result and still depending on the available G-actin-ATP concentration, actin filaments will undergo treadmilling, an equilibrium phase characterized by a balance of actin monomer polymerization at fast growing ends and actin monomer depolymerization at slow growing ends. G-actin needs to be loaded with ATP to enable the formation of F-actin. *In vivo* the ATP concentration in cells is sufficiently high to favor G-actin-ATP formation and actin polymerization. There are other actin regulatory proteins present which positively or negatively affect this polymerization process. For example, profilin favors an exchange of ATP for ADP. Since these favorable interactions are not present *in vitro*, actin needed to be primed with ATP in a separate reaction prior to SPR measurements.

7.1.1 Kinetic Experiments

Actin was immobilized on the CM5 sensor surface using the amine coupling (see 5.1). actin was also injected as the analyte in a series with increasing concentrations. Before injection, actin was primed with 10 mM ATP for two hours in the presence of 2 mM $MgCl_2$ and 100 mM KCl, conditions favoring actin polymerization. Actin concentrations used were below the critical concentration for actin polymerization for the fast-growing end (3μM). This concentration range permitted the evaluation of actin-actin interactions with little or no polymerization into actin filaments thus allowing a focus on the

nucleation phase of actin polymerization. G-actin-ATP concentrations ranged from 3 μM to 30 nM was and were injected at a flow rate of 30μl/min over a 3min time period. Dissociation was monitored for 4 min after the end of injection. The experiment was carried out using HBS-EP buffer supplemented with 2mM $MgCl_2$, 100 mM KCl and 10 mM ATP. 10 mM Glycine-HCl (pH 3.5) was used as a regeneration solution after each cycle.

7.1.2 Results and Discussion

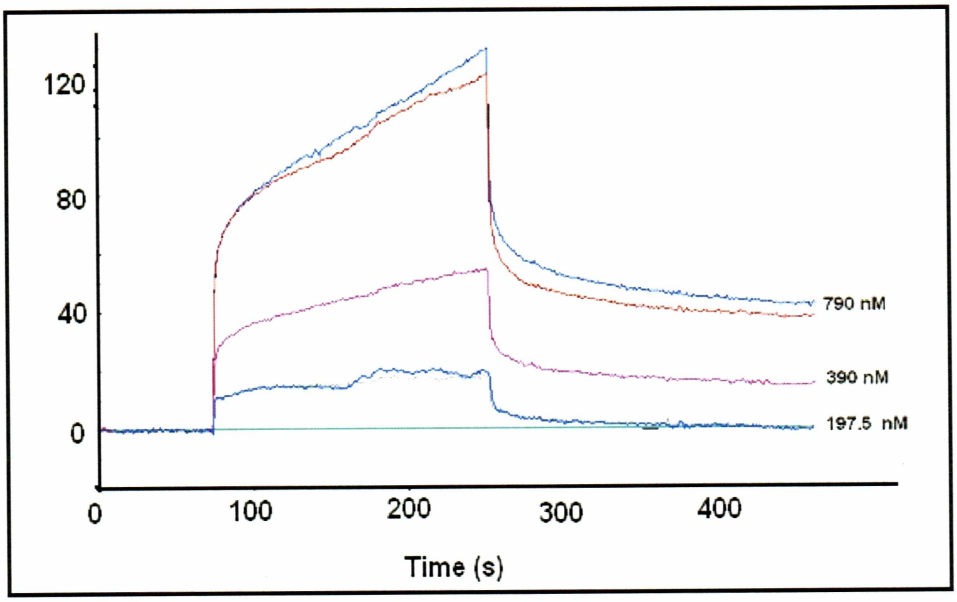

Figure 7.1 Actin-Actin Binding Interaction Below Critical Concentration.

Figure 7.1 demonstrates the raw data of actin-actin binding interactions. G-actin-ATP in solution passing over actin immobilized onto the sensor chip surface exhibits a concentration dependent binding. At low concentrations, the association rate is slower and a small maximum binding response with a distinct saturation phase is detected. At higher concentrations, association even at similar rates generate higher maximum binding responses but no saturation phase is detectable. Thus, different patterns of binding traces

represent different affinity constants for the interaction at different G-actin-ATP concentration.

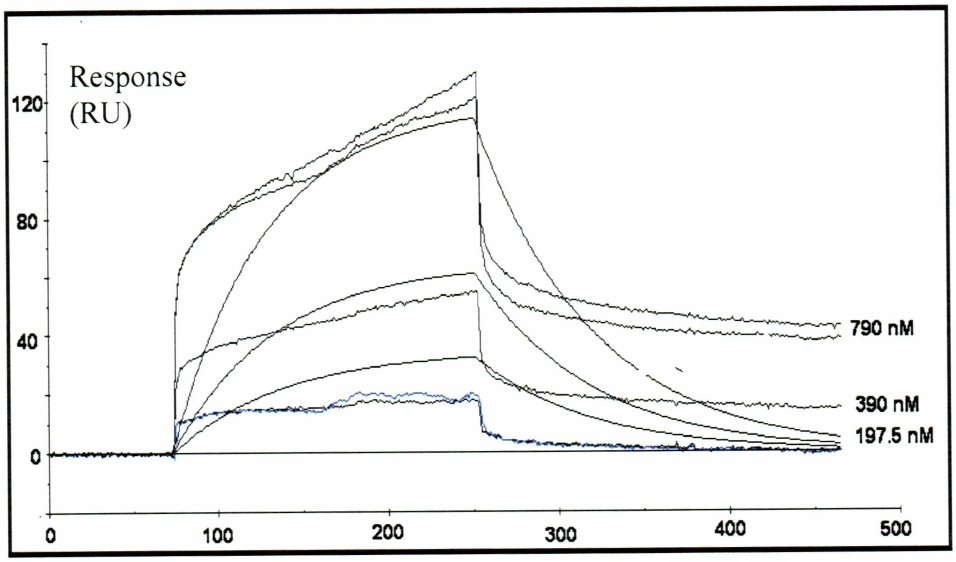

Figure 7.2 Actin-Actin Binding Data Analysis with 1:1 Binding Model

Initially we attempted to analyze this data with the 1:1 binding model smilar to the actin-DNase I interaction. This model assumes that protein A binds reversibly to protein B with an assocation rate constant k_a and a dissociation rate constant k_d to form the complex AB. Figure 7.2 demonstrates the analysis of actin-actin binding traces with this model. Clearly, the experimental curves do not fit at all to the mathematical rate equation of 1:1 binding model as revealed by a chi^2 value of 71. Therefore, actin-actin binding interactions below the critical concentration of actin polymerization do not follow a simple 1:1 binding mechanism.

Binding of a single G-actin-ATP molecule to another G-actin-ATP molecule represents exactly the initial phase of actin polymerization (see chapter ONE). The nucleation phase and the nucleation of actin polymerization does not reflect a 1:1 reversible binding But is rather a stepwise process where one G-actin-ATP monomer

binds to the previous one, which has bound the ligand and so forth. Potentially, each incoming monomer creates an additional interaction surface for the next actin monomer until an optimal configuration is achieved that cannot be surpassed by additional monomer binding. This phenomenon is also known as cooperativity and exists in many complex biological systems. Considering the arrangement of actin monomers in an actin filament, at least three actin subunits interact with the forth one. As one turn of the helix is completed by approximately 3.7 monomers, for any oncoming monomers the surface presented for binding remains the same and hence the rest of the monomers in the actin filament same kinetics. A potential cooperation for actin nucleation should be included in a binding model. This theory was implicated in the kinetic equation and a model (Nucleation Model) was created, which takes into account those particular steps and individual rates. This model considers multiple binding steps with individual kinetics for the first three subunit additions and identical kinetics parameters thereafter. As expected, this "Nucleation" model fitted well our experimental data traces as shown in figure 7.3.

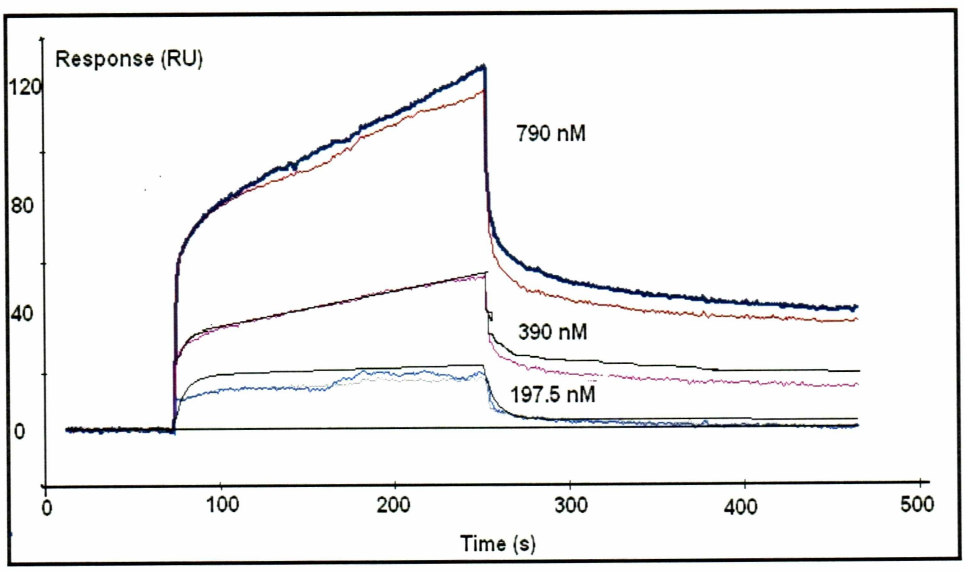

Figure 7.3 Actin-Actin Binding Interaction Below Critical Concentration Analyzed by Nucleation Model

As Figure 7.3 shows, the Nucleation model fits perfectly well to the experimental binding curves with a chi^2 value in the range of 1.3-1.7. The theoretical maximum for the first monomer was calculated as 42 RU while that for the second monomer was calculated as 124 RU. The excellent fit of sensograms to the Nucleation model confirms that interactions during actin nucleation follow a sequential binding interaction mechanism. As actin polymerization at high G-actin-ATP concentrations does not reach saturation, the later part of association curves reflects likely polymerization. After addition of one G-actin-ATP monomer to a filament end there is new existing filament end. It rather forms a straight increasing RU resonse as every incoming G-actin_ATP monomer provides a new end for an F-actin molecule. Kinetic parameters were extracted from the analysis are as follows (n=3, SD +/- 0.01).

Association rate constant for first monomer $k_a = 7.5x10^3\ \mu M^{-1}sec^{-1}$

Dissociation rate constant for first monomer $k_d = 0.256\ sec^{-1}$

Association rate constant for second monomer $k_a = 6.66x10^3\ \mu M^{-1}sec^{-1}$

Dissociation rate constant for second monomer $k_d = 1.82x10^{-3}\ sec^{-1}$

7.1.3 Conclusions

We have established conditions (actin immobilization, ATP loading, ionic conditions), which enable of the use of SPR to study actin-actin interaction both during the nucleation phase as well as during the polymerization phase. Analysis of these interactions revealed that actin nucleation is a cooperative event with the binding affinity increasing for each newly added subunit. The average dissociation rate constant of the second monomer was found to be much lower ($k_d=1.82x10^{-3}\ sec^{-1}$) as compared to the dissociation rate constant for first monomer ($k_d=0.256\ sec^{-1}$). After addition of the forth actin monomer, our experiments indicate that the system reaches polymerization kinetics. Presently, there is no kinetic data reported addressing the initial stages of actin polymerization by direct binding assays. Few groups have simulated models describing actin dynamics and have predicted kinetic parameters of actin-actin binding based on those models. Grazi et al, 1983 have reported an average dissociation rate constant of $6x10^{-3}\ sec^{-1}$ for actin nuclei at

14 μM G-actin_ATP concentrations. This data was obtained using viscosity measurements. Sept and McCammon (2001) have performed computer simulations and free energy calculations to determine the kinetics of actin nucleation using a series of Brownian dynamics simulation. These theoretical calculations yielded an association rate constant of 1.63×10^8 $\mu M^{-1} sec^{-1}$ for the first monomer while the association rate constant for the second monomer was predicted as 1.3×10^3 $\mu M^{-1} sec^{-1}$. The dissociation rates constant were calculated by combining the binding free energies and the association rate constant. The k_d for the first monomer was reported to be 1.23 sec^{-1} while for the second monomer was determined to be in the range 0.77-23.5 sec^{-1} depending upon the three dimensional structure of the nucleus in the space. The difference between the values reported by these groups and our data can most likely be attributed to the difference between simulation and actual experimental data as achieved in real time using SPR technology.

7.2 Actin-Actin Interactions under Oxidizing Conditions

As discussed in chapter three, actin is one of the cellular targets most susceptible to oxidation. There are specific cysteines (for instance Cys374) and methionines that are modified as a result of oxidative stress depending upon the duration and intensity of oxidation. Oxidation is thought to have altered actin structure and eventually its function. Oxidation can have mild modulatory effect or drastic adverse effect on kinetics of actin polymerization as well as interactions with actin-binding proteins. We attempted to understand the effect of oxidation of actin on the kinetic parameters of actin polymerization.

7.2.1 Kinetic Experiment

In these experiments, only actin injected as our analyte was exposed to oxidations. First, actin was incubated with ATP in HBS-EP with 2 mM $MgCl_2$ and 100 mM KCl for 2 hr at RT. Next, this solution was oxidized with various concentrations of H_2O_2 for different time periods. Finally, peroxide was removed either by addition of the catalytic

antioxidant 50 μM Manganese meso-Tetrakis (4-Benzoic Acid) Porphyrin (MnTBAP) or by buffer exchange in a spin column. MnTBAP is a synthetic metalloporphyrin, which catalyzes the dismutation of superoxide, hydrogen peroxide and scavenging of peroxynitrite.

7.2.2 Results and Discussion

Exposure of actin to 100 μM H_2O_2 for 20 min and subsequent incubation with 50 μM MnTBAP for 20 min resulted in no binding of oxidized actin (data not shown). Most likely oxidation conditions (100μM peroxide for 20 min) were too harsh and completely abolished the ability of actin to polymerize. Moreover, we found that MnTBAP affect immobilized actin on the sensor chip surface. After MnTBAP injection, the amount of immobilized actin on the chip was found to be decreasing over time suggesting that MnTBAP caused a chemical reaction with bound actin and subsequent release.

In a next set of experiments, actin oxidation was followed by a buffer exchange to ensure no residual peroxide in the injected analyte solution would alter immobilized actin on the sensor chip surface. To measure significant actin-actin interactions after oxidation, it was necessary to increase concentration of oxidized actin in the analyte solution almost 100 fold (see figure 7. 4) compared to unoxidized actin. Analysis of RU responses revealed that 100 μM oxidized actin was required to generate a similar RU response as obtained with 1 μM non-oxidized actin.

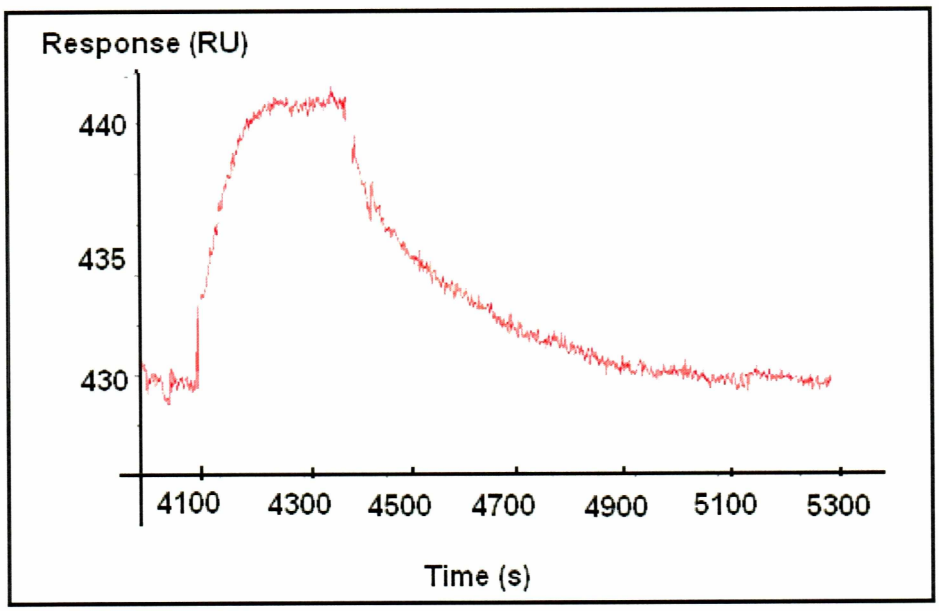

Figure 7.4 Binding Interaction of Actin with Unmodified Actin. Binding of 1 μM unoxidized actin generates about 10 RU response.

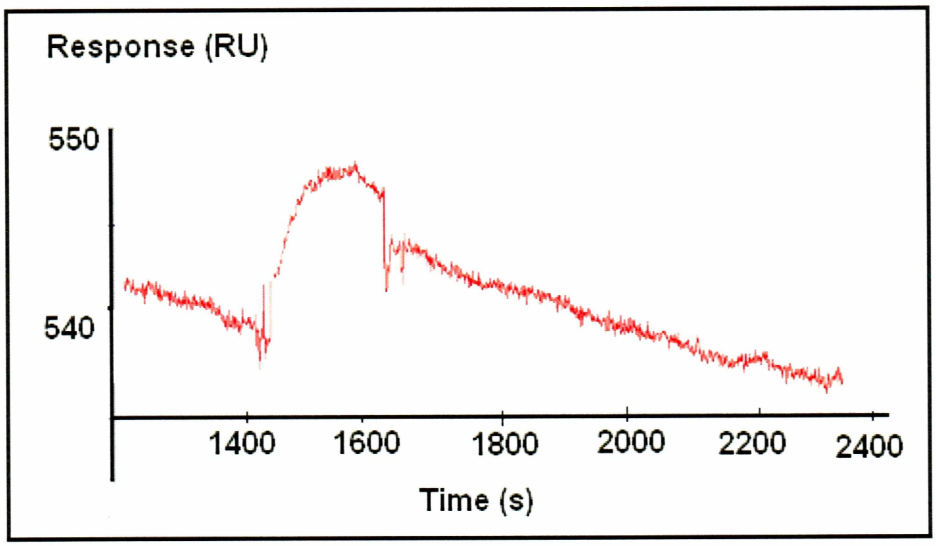

Figure 7.5 Binding Interaction of Actin with Oxidized Actin. 100 μM oxidized actin required to generate similar Response (10RU) as generated by 1 μM unoxidized actin.

7.2.3 Conclusions

Oxidation affects the structure and function of actin. It is reflected in kinetic parameters of actin polymerization as detected by SPR. H_2O_2 was used as the oxidizing agent in those experiments. This could potentially result in dissociation of ATP from G-actin-ATP or it can alter ATP binding to G-actin. The oxidant has to be eliminated after treatment so as to prevent any effect of residual oxidant on the sensor surface. Here we used a spin column to separate MnTBAP and modified actin. Purification can also be done with subsequent protein assay. Oxidation with peroxide vs. superoxide might have distinct effect. Superoxide is shown to increase the pool of F-actin in endothelial cells following hypoxia resulting in profound reorganization of the actin cytoskeleton (Crawford et al, 1996). These oxidizing conditions might reflect different kinetics of treated actin with SPR. Our experiments do not reveal anything about structural changes in actin as a result of oxidation but considering the literature and our binding data we could speculate this concentration most probably resulted in a chemical change in the Cys 374 environment and oxidizes methionines at position 44, 47 and 355 (Dalle-Donne et al, 2001). The most likely explanation for the reduction in affinity of actin for incoming G-actin molecules is the alteration of surface properties as a result of residual oxidant in the solution. As discussed earlier in this chapter the actin-actin binding interaction was studied at actin concentrations ranging from 30nM to 3 μM. The binding assay performed using this range of oxidized actin did not reveal a nucleation step. Nucleation was not seen even at high actin concentration. Both the association and dissociation phases of the traces look more like a 1:1 binding interaction. The average (n=6, +/- 0.012) association rate constant was found to be a little slower (3.8×10^3 $\mu M^{-1} sec^{-1}$) than that for the first monomer addition (7.5×10^3 $\mu M^{-1} sec^{-1}$). The average (n=6, +/-0.012) dissociation rate constant (0.78×10^{-3} sec^{-1}) however was found to be in between the dissociation of the first (0.256 sec^{-1}) and the second monomer dissociation (1.82×10^{-3} sec^{-1}) in the nucleation step.

CHAPTER EIGHT

Overall Conclusions

In this project, Surface Plasmon Resonance was employed for the first time to study actin-actin interactions. Establishing the proper conditions required careful analysis of buffer conditions and ATP loading as well as an injection protocol. Actin needs to be in optimal buffer conditions with sufficient ATP (2mM) and sufficient ions (2mM $MgCl_2$ and 100 mM KCl. Actin need to be primed with ATP by incubating with freshly prepared ATP solution (5-10 mM) for about two hours. As a result of multiple possible orientations on the surface of the sensor chip actin immobilized exhibit less activity on surface than expected 100 % activity. As our key result, we were able to obtain real-time measurements of the kinetic parameters of actin-actin interaction. The SPR approach overcomes the need of labeling actin for detection purposes. In contrast to solution studies, SPR allows one to measure the kinetic parameters of individual actin subunit interactions as opposed to solution studies, which provides average kinetic parameters of filament formation. SPR is useful to study interactions of actin both with itself and with other actin binding proteins.

We have developed a unique assay for actin nucleation that represents a good model for cellular events. This project results in the determination of the kinetic parameters of the nucleation phase of actin polymerization. These parameters were so far only speculative through mathematical modeling since actual real time interactions measurements have not been performed. SPR overcomes the need to consider the overall polymerization rate and enables a clear distinction among different phases of actin polymerization focusing on individual actin-actin subunit interactions. This in turn can be very useful to study actin modulation during specific phases of actin filament dynamics including nucleation, elongation, steady state, and depolymerization. It provides an excellent method to study pathological or pathophysiological modifications of actin or

actin regulatory proteins, which might specifically affect nucleation step without affecting rest of the phases. Initial studies demonstrated that oxidation of actin had negative affects on the affinity of actin-actin subunit binding. This data has implications for not only oxidation but also the effects of regulatory proteins and potentially drugs on actin polymerization. Similar experiments could also be used to identify toxins altering actin kinetics. The effects of nearly any actin modulatory process on nucleation could be studied using this system.

.

CHAPTER NINE

Future Directions

This project revealed the nucleation step of actin polymerization, which is a great advancement. Further studies should be able to determine kinetic parameter of actin filament elongation and actin filament depolymerization. These studies will have take to focus on actin-actin interactions above the critical concentration of free actin subunits. In analogy, binding parameters of ADP to actin can be evaluated and contrasted to obtained values of ATP-actin interactions.

Actin capping proteins or specific pharmacological agents (cytochalasin) can be used with immobilized actin on the chip to focus on one specific end of growing filament such as the fast growing or slow growing ends. For example cytochalasin can be used to cap the fast growing end of the filament thus enabling only interaction at the slow-growing end of the filament

The effect of actin oxidation can extensively be studied with specific oxidizing conditions including the effects of different buffer conditions and ATP concentrations on susceptibility of actin to oxidation. Oxidation can also be studied more specifically with regard to the oxygen radical utilized in actin oxidation. Moreover, actin oxidation under physiological conditions could be addressed by isolating actin from cells exposed to stimuli known to oxidize actin. These studies need to be combined with detailed biochemical studies on the residues within the actin subunit that are oxidized in the context of actin structure and interaction surfaces altered.

Finally, SPR would allow investigating binding interactions of actin with other actin binding proteins pivotal to regulated actin filament dynamics *in vivo*. For example it would be very important to see how Arp2/3 facilitates nucleation of actin polymerization

and if kinetics of this interaction is adversely affected oxidative stress conditions. Profilin plays a key role in the recruitment of actin subunits for filament growth. Similarly, ADF/Cofilin is key to filament growth. It would be interesting to characterize those binding interactions in real time using SPR.

References

Adams S., Green P., Claston E., Simcox S., Williams M. V., Waish K., Leeuwenburgh C., 2001, Reactive Carbonyl Formation by Oxidative And non-Oxidative Pathways, Frontiers in Bioscience, 6, 17-24.

Aksenov M., Aksenova M., Butterfield, D., Geddes J., Markesbery W., 2001, Protein Oxidation in the Brain in Alzheimer's Disease, Neuroscience, 103, 373–383.

Banan A., Fitzpatrick L., Zhang Y., Keshavarzian A., 2000, OPC-compounds Prevent Oxidant-induced Carbonylation and Depolymerization of the F-actin Cytoskeleton and Intestinal Barrier Hyperpermeability, Free Radical Biology and Medicine, Volume 30, 3, 287-298.

Banan A., Zhang Y., Losurdo J., Keshavarzian A., 2000, Carbonylation and Disassembly of the F-actin Cytoskeleton in Oxidant Induced Barrier Dysfunction and its Prevention by Epidermal Growth Factor and Transforming Growth Factor α in a Human Colonic Cell Line, Gut. 46, 830–7.

Biacore Instrument Handbook, Biacore Inc., Uppasala Sweeden, 2002.

Biacore Application Handbook, Biacore Inc., Uppasala Sweeden, 2002.

Berlett B. S., and Stadtman E.R., 1997, Protein Oxidation in Ageing, Disease, and Oxidative Stress, The Journal of Biological Chemistry, Volume 272, 33, Issue August 15, 20313-20316.

Bremer A. and Aebi U., 1992, The Structure of the F-actin Filament and the Actin Molecule, Current Opinion in Cell Biology, 4, 20-26.

Carlier M. F., and Pantaloni D., 1997, Control of Actin Dynamics in Cell Motility. Journal of Molecular Biology, 269, 459–467.

Christman M., Morgan R., Jocobson F., Ames B., 1985, Positive Control of Regulation for Defenses against Oxidative Stress and some Heat-shock Proteins in Salmonella typhi, Cell, 41: 753-762.

Crawford L. E., Milliken E. E., Irani K., Zweier J. L., Becker L. C., Johnson T. M., Eissa N. T., Crystal R. G., Finkel T., Goldschmidt-Clermont P. J., 1996, Superoxide-mediated Actin Response in Post-hypoxic Endothelial Cells, Journal of Biological Chemistry, Volume 271, # 43, 26863-26867.

Dalle-Donne I., Carini M., Vistoli G., Gamberoni L., Giustarini D., Colombo R., Facino R., Rossi R., Milzani A., Aldini G., 2007, Actin Cys374 as a Nucleophilic Target of α, β–unsaturated Aldehydes, Free Radical Biology and Medicine, Volume 42, 583-598.

Dalle-Donne I., Aldini G., Carini M., Colombo R., Rossi R, Milzani A., 2006, Protein Carbonylation, Cellular Dysfuntion, and Disease Progression, Journal of Cellular and Molecular Medicine, 389-406.

Dalle-Donne I., Scaloni A., Giustarini D., Cavarra E., Tell G., Lungarella G., Colombo R., Rossi R., Milzani A., 2005, Proteins as Biomarkers of Oxidative/ Nitrosative Stress in Diseases: The Contribution of Redox Proteomics, Mass Spectrometry Reviews, 24, 55-99.

Dalle-Donne I., Giustarini D., Rossi R., Colombo R., Milzani A., 2003, Reversible S-Glutathionylation of Cys 374 Regulates Actin Filament Formation by Inducing Structural Changes in the Actin Molecule, Free Radical Biology and Medicine, 34, 23–32.

Dalle-Donne I., Rossi R., Giustarini D., Gagliano N., Simplicio D., and Colombo R., 2002, Methionine Oxidation as a Major Cause of the Functional Impairment of Oxidized Actin, Free Radical Biology and Medicine, Volume 32, 9, 927–937.

Dalle-Donne I., Rossi R., Giustarini D., Gagliano N., Lusini L., Milzani A., Simplicio P., and Colombo R., 2001, Actin Carbonylation: From a Simple Marker of Protein Oxidation to Relevant Signs of Severe Functional Impairment, Free Radical Biology and Medicine, Volume 31, 9, 1075-1083.

Dalle-Donne I., Rossi R., Milzani A., di Simplicio P., Colombo R., 2001, The Actin Cytoskeleton Response to Oxidants: From Small Heat Shock Protein Phosphorylation to Changes in the Redox State of Actin Itself, Free Radical Biology and Medicine, Volume 31, 1624–1632.

Degen J., Neubauer M., Degen S., Seyfried C., Morris D., 1983, Regulation of Protein Synthesis in Mitogen-activated Bovine Lymphocytes, Analysis of Actin-specific and Total mRNA Accumulation and Utilization, The Journal of Biological Chemistry, Volume 258, 20, 12153-12162.

Droge W., 2003, Oxidative Stress and Aging, Advanced Experimental Medicine and Biology, 543,191–200.

Fiaschi T., Cozzi G., Raugei G., Formigli L., Ramponi G., 2006, Redox Regulation of β-Actin during Integrin-mediated Cell Adhesion, The Journal of Biological Chemistry, Volume 281, 32, 22983-22991.

Fratelli M., Gianazza E., and Ghezzi P., 2004, Redox Proteomics: Identification and Functional Role of Glutathionylated Proteins, Expert Review in Proteomics, 1(3), 365-376.

Ghezzi P. & Bonetto V., 2003, Redox Proteomics: Identification of Oxidatively Modified Proteins, Proteomics, 3, 1145-1153.

Goldschmidt-Clermont P. J., Moldovan L., 1999, Stress, Superoxide, and Signal Transduction, Gene Expression, 7, 255–260.

Grazi E., Ferri A., Cino S., 1983, The Polymerization of Actin, a Study of the Nucleation Reaction, Biochemistry Journal, 213, 727-732.

Groemping Y and Rittinger K., 2005, Activation and Assembly of the NADPH Oxidase: a Structural Perspective, Review in Biochemistry Journal, 386, 401–416.

Hambly B. D., Barden J. A., Miki M., and Remedios C. G., 1972, Structural and Functional Domains on Actin, Bioassays Review Articles, Volume 4, 3, 124-128.

Hirota K., Murata M., Sachi Y., Nakamura H., Takeuchi J., Mori K., and Yodoi J., 1999, Distinct Roles of Thioredoxin in the Cytoplasm and in the Nucleus. A Two-step Mechanism of Redox Regulation of Transcription Factor NF- κB, Journal of Biological Chemistry, 274: 27891–27897.

Holmes K. C. and Kabsch W., 1991, Muscle Proteins: Actin, Current Opinion in Structural Biology, 1, 270-280.

Kong S. K., Yim M. B., Stadtman E. R., Chock P. B., 1996, Peroxynitrite Disables the Tyrosine Phosphorylation Regulatory Mechanism: Lymphocyte-Specific Tyrosine Kinase Fails to Phosphorylate Nitrated cdc2 (6-20) NH2 Peptide, Proceeding National Academy of Science USA, 93: 3377–3381.

Lassing I., Schmitzberger F., Bjornstedt M., Holmgren A., Norddluncd P., Schutt C. E., and Lindberg U., 2007, Molecular and Structural Basis for Redox Regulation of β–Actin, Journal of Molecular Biology, 370, 331-348.

Lodish H., Arnold B., Kaiser C., Krieger M., Scott M., Bretscher A., Ploegh H., Matsudaira P., Molecular Cell Biology, Fifth Edition, 2005, W. H. Freeman Publication, ISBN 978-0-716-77601-7.

Luo 2002, Actin Cytoskeleton Regulation in Neuronal Morphogenesis and Structural Plasticity, Annual Review in Cell and Developmental Biology, 18, 601-635.

Milzani A., Dalle-Donne I., Colombo R., 1997, Prolonged Oxidative Stress on Actin, Archives of Biochemistry and Biophysics, 339, 267–274.

Moldovan L., and Moldovan N. I., 2004, Oxygen Free Radicals and Redox Biology of Organelles, Histochemistry and Cell Biology, 122, 395-412.

Moldovan L., Moldovan N. I., Sohn R. H., Parikh S. A., Goldschmidt-Clermont P. J., 2000, Redox Changes of Cultured Endothelial Cells and Actin Dynamics, Circulation Research, 86, 549–557.

Moldovan L., Irani K., Moldovan N. I., Finkel T., Goldschmidt-Clermont P. J., 1999, The Actin Cytoskeleton Reorganization Induced by Rac1 Requires the Production of Superoxide, Antioxidant Redox Signaling, 1,29–43.

Moldovan L., and Goldschmidt-Clermont P. J., 1998, Of Proteins, Redox States and Living Things, Dynamical Networks in Physics and Biology, Springer, Berlin Heidelberg New York, 51–66.

Moldovan N. I., Milliken E. E., Irani K., Chen J., Sohn R. H., Finkel T., Goldschmidt-Clermont P. J., 1997, Regulation of Endothelial Cell Adhesion by Profilin, Current Biology, 7, 24–30.

.

Myszka D., 2000, Kinetic, Equilibrium, and Thermodynamic Analyses of Macromolecular Interactions with Biacore, Methods in Enzymology, 323, 325-340.

O'Shannessy, 1992, Determination of Rate and Equilibrium Binding Constants for Macromolecular Interactions Using Surface Plasmon Resonance: Use of Nonlinear Least Squares Analysis Methods, Analytical Biochemistry, 212, 457-460.

Pastore A., Tozzi G., Gaeta L. M., Bertini E., Serafini V., Di Cesare S., Bonetto V., Casoni F., Carrozzo R., Federici G., Piemonte F., 2003, Actin Glutathionylation Increases in Fibroblasts of Patients with Friedreich's Ataxia: a Potential Role in the Pathogenesis of the Disease, Journal of Biological Chemistry, 278, 42588–42595.

Pietro G. and Bonetto V., 2003, Redox Proteomics: Identification of Oxidatively Modified Proteins, 3, 1145-1153.

Pollard, 1986, Rate Constants for the Reactions of ATP- and ADP-Actin with the Ends of Actin Filaments, the Journal of Cell Biology, Volume 103, 2747-2754.

Pollard T., Blanchoin L., Mullins R., 2000, Molecular Mechanisms Controlling Actin Filament Dynamics in Non-muscle Cells, Annual Review of Biophysics and Biomolecular Structure, Volume 29, 545-576

Pollard T. D., 1986, Assembly and Dynamics of the Actin Filament system in Nonmuscle Cells, Journal of Cell and Biochemistry, 31, 87–95.

Pollard T. D., 1988, Macromolecular Motion in the Actin Cytoskeleton Depends on Dynamic, Low-affinity Interactions, Signal Transduction in Cytoplasmic Organization and Cell Motility, New York, 263–269.

Pollard T. D., and Cooper J. A., 1986, Actin and Actin-Binding Proteins: A Critical Evaluation of Mechanisms and Functions, Annual Review of Biochemistry, 55, 987–1035.

Powell S. R., Gurzenda E. M., and Wahezi S. E., 2001, Actin is Oxidized During Myocardial Ischemia, Free Radical Biology and Medicine, Volume 30, 10, 1171-1176.

Sept D., and McCammon J. A., 2001, Thermodynamics and Kinetics of Actin Filament Nucleation, Biophysical Journal, Volume 81, 667-674.

Stadtman E. R., 2006, Protein Oxidation and Aging, Free Radical Research, 40 (12), 1250-1258.

Tamura M., Kai T., Tsunawaki S., Lambeth J. D., Kameda K., 2000, Direct Interaction of Actin with p47 (phox) of Neutrophil NADPH Oxidase, Biochemistry and Biophysics Research, 276, 1186–1190.

Thannickal V. J., and Fanburg B. L., 2000, Reactive Oxygen Species in Cell Signaling, American Journal Physiology Lung Cell Molecular Physiology, 279, L1005-L1028.

Vanderkerckhove J., and Weber K., 1984, Chordate Muscle Actin Differ Distinctly from Invertebrate Muscle Actins, Journal of Molecular Biology, Volume 179, 391-413.

Vidali L., McKenna S., Hepler P., 2001, Actin polymerization is Essential for Pollen Tube Growth, Molecular Biology of the Cell, Volume 12, 2534–2545.

Wriggers and Schulten, 1997, Stability and Dynamics of G-actin: Back Door Water Diffusion and Behavior of a Subdomain 3/4 Loop, Biophysical Journal, Volume 73, 624-639.

Xu J., Schwarz W. H., Kas J. A., Stossel T. P., Janmey P. A., Pollard T. D., 1998, Mechanical Properties of Actin Filament Networks Depend on Preparation, Polymerization Conditions, and Storage of Actin Monomers, Journal of Biophysics, 74, 2731–2740.